

ANKARA YILDIRIM BEYAZIT UNIVERSITY
GRADUATE SCHOOL OF NATURAL AND APPLIED SCIENCES



TiO₂ BASED DYE SENSITIZED SOLAR CELLS
OBTAINED BY SOL-GEL METHOD

M.Sc. Thesis by

Zikreddin Kerem YILDIZ

Department of Energy Systems Engineering

January, 2018

ANKARA

**TiO₂ BASED DYE SENSITIZED SOLAR CELLS
OBTAINED BY SOL-GEL METHOD**

A Thesis Submitted to

The Graduate School of Natural and Applied Sciences of

Ankara Yıldırım Beyazıt University

**In Partial Fulfillment of the Requirements for the Degree of Master of Science
in Energy Systems Engineering, Department of Energy Systems Engineering**

by

Zikreddin Kerem YILDIZ

January, 2018

ANKARA

M.Sc. THESIS EXAMINATION RESULT FORM

We have read the thesis entitled “**TiO₂ BASED DYE SENSITIZED SOLAR CELLS OBTAINED BY SOL-GEL METHOD**” completed by **ZİKREDDİN KEREM YILDIZ** under the supervision of **PROF. DR. ABDULLAH YILDIZ** and we certify that in our opinion it is fully adequate, in scope and in quality, as a thesis for the degree of Master of Science.

Prof. Dr. Abdullah YILDIZ

Supervisor

Doç. Dr. Sinan KIVRAK

Jury Member

Prof. Dr. Selim ACAR

Jury Member

Prof. Dr. Fatih Vehbi ÇELEBİ

Director

Graduate School of Natural and Applied Sciences

ETHICAL DECLARATION

I hereby declare that, in this thesis which has been prepared in accordance with the Thesis Writing Manual of Graduate School of Natural and Applied Sciences,

- All data, information and documents are obtained in the framework of academic and ethical rules,
- All information, documents and assessments are presented in accordance with scientific ethics and morals,
- All the materials that have been utilized are fully cited and referenced,
- No change has been made on the utilized materials,
- All the works presented are original.

Date: January, 2018

Signature:.....

Name & Surname: Zikreddin Kerem YILDIZ

ACKNOWLEDGMENTS

I ask to state my profound thanks to anyone who has help me, irrespective of whether there is more or less to me during this thesis work. I am deeply grateful to Prof. Dr. Abdullah YILDIZ who helped by sharing his knowledge and skill with me so that I can do research on the current issue, directing it in the stage of experiment correctly with the domination of the subject, encouraging me in the thesis writing phase and giving me all kinds of support

Furthermore, Ph.D.Student Abdullah ATILGAN, Aycan ATLI, Mohammed SBETA who help me by giving information about the devices and their usage, also especially in the experimental phase, giving me all kinds of support .

Eventually, my life giving me every opportunity, I always have the memories with me and As I feel the unlimited support of the family every moment of my life, I must emphasize what I feel while writing my thesis. A large part of this success was with their help.

Thank You.

2018, 03 January

Zikreddin Kerem YILDIZ

TiO₂ BASED DYE SENSITIZED SOLAR CELLS OBTAINED BY SOL-GEL METHOD

ABSTRACT

In this study, spin-coated titanium dioxide films were deposited with different coatings cycles (five cycles, ten cycles, fifteen cycles) on fluorine-doped tin oxide coated glass substrates. The effects of thickness and different dyes on the efficiency of dye sensitized solar cells (DSSCs) were investigated with applying three different sensitizer dyes which are black mulberry (*morusnigra*), madder (*rubiatictorum*) fruits, and eosin y . The TiO₂ films were characterized by X – Ray diffraction (XRD), UV– Visible and Atomic Force Mikroskopy (AFM). In the process of forming the DSSCs structure, , the electrolyte solution containing redox reactions for the regenerating of the dye was deposited between the working electrode and the counterelectrode. The photovoltaic conversion performance parameters of the fabricated DSSC were measured under standart test conditions. The best conversion efficiency was obtained for the thickest TiO₂ film that loaded with black mulberry dye.

Keywords: TiO₂ thin film, sol-gel, spin-coating technique, thickness, dye-sensitized solar cells

TiO₂ BAZLI BOYAYA DUYARLI GÜNEŞ PİLLERİNİN SOL-GEL YÖNTEMİ İLE ELDE EDİLMESİ

ÖZ

Yapılan bu çalışmada; titanyum dioksit filmler, spin kaplama tekniğiyle farklı sayıda ve periyodik olarak (beş, on ve onbeş döngü) filorun katkılı kalay oksit kaplı camın üzerine kaplandı. Kalınlığın ve dut, kök boyası ve eozin y gibi üç farklı boyanın, boya duyarlı güneş pilinin verimliliğine etkisi araştırıldı. Filmler X-ışını kırınımı, UV-görünür bölge absorpsiyonu ve atomik kuvvet mikroskopu kullanılarak karakterize edildi. Boya duyarlı güneş pilinin oluşturulması sürecinde, boyanın tekrar üretilmesi için, indirgenme, yükseltgenme reaksiyonlarını içeren elektrolit çözeltisi çalışma elektrodu ve karşıt elektrod arasına yerleştirildi. Üretilen boya duyarlı güneş pilinin fotovoltaj dönüşüm performans parametreleri standart test koşulları altında ölçüldü. En iyi dönüşüm verimliliği dut boyası ile boyanan en kalın filmde elde edildi.

Anahtar Kelimeler: TiO₂ ince film, sol-jel, spin-kaplama tekniği, kalınlık, boya duyarlı güneş pilleri

CONTENTS

M.Sc. THESIS EXAMINATION RESULT FORM	ii
ETHICAL DECLARATION	iii
ACKNOWLEDGMENTS.....	iv
ABSTRACT	v
ÖZ	vi
NOMENCLATURE	ix
LIST OF TABLES.....	xii
LIST OF FIGURES	xiii
CHAPTER 1- INTRODUCTION	1
CHAPTER 2 – DYE SENSITIZED SOLAR CELLS	4
2.1 Architecture and Basic functioning steps of DSSCs	4
2.1.1 Parts of DSSCs.....	5
2.1.2 Basic functioning steps of DSSCs	7
2.1.3 Performance parameters affecting the efficiency of DSSCs	10
2.1.4 The Basic equivalent circuit of DSSC.....	13
2.1.5 Literature Review.....	15
CHAPTER 3 – FABRICATION AND CHARACTERIZATION DEVICES..	17
3.1 Cutting, cleaning and measuring the TCO.....	17
3.2 Preparation of solution and deposition of TiO ₂ on TCO	18
3.3 Dye Sensitiser Extraction and Preparation	21
3.4 Preparation of electrolyte	23
3.5 Preparation of Counter Electrode	23
3.6 DSSC Fabrication.....	23
3.7 Characterization Methods Devices Of DSSCs.....	24
3.7.1 X-ray Diffraction (XRD).....	24
3.7.2 Atomic Force Microscope (AFM)	27
3.7.3 UV-Vis Spectroscopy.....	29
3.7.4 Solar Simulator	30
CHAPTER 4 - RESULTS	32
4.1 Structural Results	32

4.2 Morphological Results	33
4.3 Optical Results	34
4.4 Electrical Results	36
CHAPTER 5 – DISCUSSION AND CONCLUSION	39
REFERENCES	42
CURRICULUM VITAE	49



NOMENCLATURE

AFM	Atomic force microscopy
AM 1.5 G	Incident air mass 1.5 global spectrum
a-Si	Amorphous silicon
CB	Conduction band
CdTe	Cadmium telluride
CIGS	Copper-indium-gallium-selenide
DSSC	Dye-sensitized solar cell
EtOH	Ethanol
FTO	Fluorine-doped tin oxide
HAc	Acetic acid
HOMO	Highest occupied molecular orbital
ITO	Indium-tin oxide
LUMO	Lowest Unoccupied Molecular Orbital
PV	Photovoltaic
Red/Ox	Reduction /Oxidation
rpm	Revolution per minute
TCO	Transparent conductive oxide
TEA	Triethylamine
TiO ₂	Titanium dioxide
TTIP	Titanium(IV) isopropoxide
UV-vis	Ultraviolet-visible
VB	Valence band
XRD	X-ray Diffraction

Symbols

J_{sc}	Short circuit current density
V_{oc}	Open circuit voltage
FF	Fill Factor
η	Efficiency
E_f	Fermi energy
$h\nu$	Light quantum
I_m	Current at the maximum power point
I_{SC}	Short-circuit current
V_m	Voltage at the maximum power point
P_i	Power of the incident light
P_{MAX}	Power at the maximum power point
S	Sensitizer
S^*	Excited energy state of the sensitizer
S^+	Oxidized state of the sensitizer
I	Output current
I_L	Photogenerated current
I_D	Diode current
I_{SH}	Shunt current
I ⁻	Iodide
I_3^-	Triiodide
R_s	Series resistance
R_{sh}	Shunt resistance
M	Molarite
λ	X-ray wavelength
d	Distance between planes in the atomic lattice

θ	angle of the incident beam with the plate
2θ	Diffraction angle
Pt	Platin
LiI	Lityum İyodür



LIST OF TABLES

Table 1 The photovoltaic parameters of DSSC obtained with different coating cycles and dyes of TiO ₂	37
--	----



LIST OF FIGURES

Figure 2. 1 Architecture of Dye Sensitize Solar Cell.....	5
Figure 2. 2 Architecture of working principle and electron conduction steps in a DSSC.....	9
Figure 2. 3 <i>J-V</i> (current density-voltage) curve.....	10
Figure 2. 4 Schematic representation of <i>V_{oc}</i>	11
Figure 2. 5 Simple equivalent circuit of DSSC	13
Figure 2. 6 Effect of <i>R_s</i> (series resistor) and <i>R_{sh}</i> (shunt).....	14
Figure 3. 1 Ultrasonic cleaner bath used in measurement.....	18
Figure 3. 2 TiO ₂ prepared by the sol-gel method	19
Figure 3. 3 Spin coater device	19
Figure 3. 4 OptoSense tube furnace used for annealing.....	20
Figure 3. 5 Coating cycle steps of TiO ₂ thin films	20
Figure 3. 6 Preparation process of dyes	21
Figure 3. 7 The dyes extracted.....	22
Figure 3. 8 Dyeing of TiO ₂ in petryls	22
Figure 3. 9 Fabrication of dye sensitized solar cell	24
Figure 3. 10 Bragg's law diagram	25
Figure 3. 11 Working Principle of X-ray Diffraction (XRD)	26
Figure 3. 12 XRD used in measurements.....	26
Figure 3. 13 Working principle of AFM	27
Figure 3. 14 AFM used in measurements	28
Figure 3. 15 Working principle of UV-Vis	29
Figure 3. 16 UV-Vis used in measurements.....	30
Figure 3. 17 Solar simulator working mechanizm.....	31
Figure 3. 18 Solar Simulator and sourcemeter used in measurements	31
Figure 4. 1 XRD spectra of TiO ₂ samples coated on FTO glasses.	32
Figure 4. 2 Surface morphology of TiO ₂ 5 cycles Working electrodes	33
Figure 4. 3 Surface morphology of TiO ₂ 10 cycles Working electrodes.....	34
Figure 4. 4 Surface morphology of TiO ₂ 15 cycles Working electrodes.....	34
Figure 4. 5 Absorbance spectra before and after dye loading of TiO ₂ with 5 coating cycles.....	35
Figure 4. 6 Absorbance spectra before and after dye loading of TiO ₂ with 10 coating cycles.....	35
Figure 4. 7 Absorbance spectra before and after dye loading of TiO ₂ with 15 coating cycles.....	36
Figure 4. 8 <i>J-V</i> curve for DSSC with different dyes for 5 coating cycles	37
Figure 4. 9 <i>J-V</i> curve for DSSC with different dyes of for 10 coating cycles	38
Figure 4. 10 <i>J-V</i> curve for DSSC with different dyes for 15 coating cycles.....	38

CHAPTER 1

INTRODUCTION

The increasing competition in high technology, industrialization, urbanization, becoming more dependent on technology in life, it takes to top the position of energy in human life. With the rise in industrialization, an increasing portion of our energy comes from non-renewable energy sources like oil and coal. As energy demand rises, these resources are exhausted and scientists are discovering the potential of renewable energy sources for the future. The use of non-renewable energy sources did not reduce the fossil fuel stock more rapidly than expected, but at the same time increased environmental pollution to catastrophic levels [1]. When non-renewable energy sources are burned, they emit pollution atmospheres, including greenhouse gases. Since it is known that it is inevitable that fossil fuels will come to an end one day, People are in search of cleaner and more sustainable energy sources that do not pollute the environment. It is also necessary to supply plenty of energy to achieve political, economic and geopolitical stability in a global sense. We get about 3×10^{24} joules / year of energy in the form of sunshine on the Earth's surface, about 104 cycles more than the world's energy consumption [2]. Thus, solar energy which is more abundant and more accessible among other renewable energy sources, as a potential alternative energy source, attracted great interest in the world after the energy crisis that took place in the 1970s [3]. The conversion of solar energy into different forms in recent years has been the essence of scientific research. Solar cells based on performance, abundance of raw materials and cost-effectiveness are classified in three generations. Today's solar energy generation is essentially based on silicon solar cell, which are called first generation solar cell. First generation solar cell have a comparatively high efficiency about 25% with costly production costs. Photovoltaic Si cells still have 86% of the solar cell market. Because they are high efficiency in spite of extreme fabricating costs [4]. Second generation solar cells were produced to reduce the cost of first generation solar cell including thin film solar cells, which have proven to be of lesser material density and more cost-effective [5]. The efficiency of first generation cells is greater than that of second generation solar cells (up to 19.6% for CIGS and up to 16.7% for CdTe cells) [6].

Moreover, the low amounts of materials used for these cells, such as indium and tellurium, make them difficult to use for mass applications [5].

In order to remove these handicaps, the work carried out was different from other solar batteries and was presented by O'Regan and Grätzel, and the dye-sensitized solar cells (DSSC) with an efficiency of 7.1% was obtained using nanocrystalline TiO_2 were aroused greatly curious and took their place as 3rd generation cells [7]. DSSCs are photonic devices that convert light into electricity under illumination, regardless of sunlight, and are based on thin film of a wide-band semiconductor oxide thin film modified by dye molecules. DSSCs can produce more energy than conventional solar cells in both indoor and outdoor in diffuse light conditions, where both light exists; they are not affected by the angular dependence of the sunlight and allow flexible, thin and light modules[5]. Just as in other PVs, the DSSC can be easily integrated into the architecture of buildings. The fact that DSSC is the only solar cell that can be made transparent by changing the sensitizing dye selection makes it a privilege. One of the biggest handicaps in the design of a dye-sensitized solar cell is the use of a very unstable liquid electrolyte at varying temperatures DSSCs have not yet been produced on a commercial scale as an option for large-scale production where higher cost, higher efficiency cells are more viable [8]. Further research is needed to increase the power conversion efficiency to transform this technology into a highly competitive option in the photovoltaic solar cell market worldwide to provide the commercialization of the DSC device. For commercial production, efficiencies of dye-sensitized solar cells higher than 15% should be obtained [9].

Chapter 1 present assessment of the demand for energy resources in a wide range, trending toward solar cells to meet energy demand, attracting features of DSSC from solar cells.

Chapter 2 includes Literature review of the developmental process of DSSC, examination of the main steps of photovoltaic conversion, solar cell architecture, working principles, evaluating of photovoltaic performance parameters, basic equivalent circuit of DSSC.

Chapter 3 describes considering the thickness of TiO_2 and dye factor how the TiO_2 thin film structure was obtained by the sol-gel spin-coating technique, preparation of working electrode, electrolyte, counter electrode and dye sensitizer extraction, fabricating of DSSC by assembling the prepared components, the devices that are utilized when characterizing the solar cell.

Chapter 4 explain experimental results obtained from characterization methods such as XRD, AFM, UV-Vis, Solar Simulator used for DSSC characterization, analysing of crystal structure of TiO_2 with XRD, surface morphology with AFM, absorbance spectrum with UV-Vis before and after dyeing, J-V characteristic curves with solar Simulator.

Chapter 5 consists of interpretation of the experimental results obtained, comparison with the results of previous scientific studies, what is the main result obtained from this study.

CHAPTER 2

DYE SENSITIZED SOLAR CELLS

In order to convert solar energy into electrical energy for large scale application, three important photovoltaic parameters require optimization: efficiency, cost and stability. Today, crystalline silicon based solar cells widely used in the market, but silicon-related issues prevent solar energy. Despite the fact that monocrystalline silicon solar cells is more efficient than other types of solar cells, the cost factor and process of toxic chemicals overshadow the advantage of high efficiency [10]. Thus, researchers have focused on overcoming the disadvantages, increasing solar energy conversion efficiency, and using nanotechnology to harvest more light energy. Professor Grätzel and his colleagues developed a solar cell that exceeded 7% in energy conversion efficiency in 1991 by accomplishing the combination of nanostructure electrodes and effective injectable dyes [7]. The manufacturing of this type of solar cells can be much cheaper than the older solid state cell designs. It can also be designed as flexible plates and mechanically resistant, and it does not require protection against small incidents such as full or tree strikes. It is stated that the dye cells perform better at a temperature close to the realistic normal working temperature that is not applicable to most PV Technologies[11]. Dye sensitized solar cells (DSSCs) make themselves different from other technologies because they use cheaper materials and exhibit higher or comparable yields than traditional Si-based solar cells under any other light source [12].

2.1 Architecture and Basic functioning steps of DSSCs

The DSSC has a sandwich type structure consisting of different functional layers;. The general architecture is formed conducting glass substrate, a mesoporous semiconductor film (working electrode), a sensitizer, an electrolyte solution with a red-ox reaction and photocathode called as counter electrode [13].

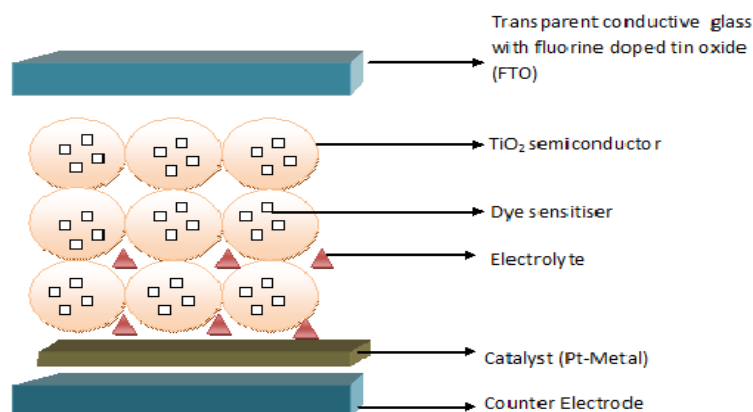


Figure 2. 1 Architecture of Dye Sensitize Solar Cell

2.1.1 Parts of DSSCs

2.1.1.1 Transparent Conductive Oxide covered with FTO coated glass

Transparent conductive glasses are often used as a substrate because of their low cost, abundant, and high optical properties. The most common one is Fluorine doped Tin Oxide (FTO). TCO substrates have to be fairly transparent to ensure the maximum absorption level of active regions of the solar spectrum. TCO should provide a compatibility between electrical conductivity and optical transparency, a careful balance between qualities is essential [14]. The TCO also operates as an optically transparent electrode that allows the photons to enter the solar cell and transport photogenerated electrons to external device terminals. For this reason, high conductivity and low UV-ray absorption are vital preconditions for the front TCO of any solar cell device. The surface of the substrate acts as a current collector and as a sealing layer between the substrate and the substrate air, providing a support to the cell itself as well [15].

2.1.1.2 Semiconductor electrode (TiO₂)

In a DSSC, Semiconductor electrode is made of a nanostructured semiconductor material attached to a transparent conductive lower substrate. The commonly used semiconductor material in DSSCs is TiO₂ due to its crystallinity, wide-band gap, and high electron mobility having extremely important transporting electron, a cheap, environment- friendly, high conductive band edge energy providing chemical

stability and abundant material [16]. The basic requirements of a suitable semiconductor film have both high surface area and high transparency. In the DSSC, mesoporous TiO₂ is used as the photoelectrode and is frequently precipitated by the sol-gel method. TiO₂ has three main phases: anatase, brookite and rutile. There are various applications of anatase and rutile phases. The optical band gap of the anatase-phase TiO₂ nanostructure is 3.2 eV, while for rutile it is 3.0 eV. Anatase-phase TiO₂ also has higher electron mobility than others. These features have played a key role for being the anatase phase is more preferred [17].

2.1.1.3 Dye Sensitizer

Dye Sensitizer is an important component to absorb the light by the DSSCs that convert the incoming light to photocurrent. Dye molecules with the appropriate molecular structure are utilized to sensitize the wide bandgap range nanostructured photoelectrode. Since the cell is a light harvesting part, it must have strong absorption in the visible spectrum. The chemical and photostable properties of the dye molecule should be good for DSSC to perform better [18]. Natural dyes are considered as a costly effective alternative for the inorganic based DSSC. In natural dyes, the plant's fruity, flowers and leaves exhibit in a different way colors from red to purple, contains different natural dyes that are extracted using simple methods and used for DSSC manufacture. As the photon in the light source hits the dye coated surface, the electrons in the dye become excited and flow into the semiconductor [19].

2.1.1.4 Electrolyte

As the electrolyte, usually I / I₃ pair are used, They participate to transfer of charge. Electrolyte has active function in solar cells by providing charge transfer between photo-electrode and counter electrode in DSSC . The electrolyte is used to reduce the amount of oxidized dye after charge injection to the minimum and then transfer the hole to the cathode [20]. When the light is converted to electricity using dye, it loses electrons and gets a positive charge. The electrolyte binds the electron to the dye and regenerates, thus opening the way for repeatability of the cycle. The electrolyte operates as a charge transport medium for the positive charge to be transmitted to the counter electrodes. Thanks to the electrolyte, since the electrochemical potential

of the counter electrode is established, output voltage of the DSSC is closely related to the red-ox reaction [21].

2.1.1.5 Counter electrode

One of the basic functions of the counter electrode is to return the electron transfer from the external circuit to the redox electrolyte. Generally, platinum is used as the most efficient and most preferred catalyst. In order to efficiently regenerate the redox couple, a platinum layer is coated on the substrate. The main function of the counter electrode is to reduce the triiodide to iodide both on the FTO coated and on surface containing electrolyte and to bring to completion the circuit. However, the surface of the counter electrode must be activated with an appropriate catalyst such as Pt. Among the reasons for preferring Pt are indicated that electrolyte during redox reactions has a high electron mobility, which can be rapidly regenerated and high electrical conductivity [22].

2.1.2 Basic functioning steps of DSSCs

2.1.2.1 Light absorption and photo-excitation

Under a light source with sufficient illumination which would excite an electron, the photon hits the TCO coated with dye molecules in the solar cell and passes through the dye sensitizer layer. This causes the photosensitizer (S) to trigger a photon as an absorbent to generate the excited state (S^*). Electrochemically formed absorption in the dye particle includes an electron passing process from HOMO (highest occupied molecular orbital) to (LUMO) the lowest unoccupied molecular orbital [23]. The equation for an excited dye is shown in (2.1).



2.1.2.2 Electron Transport

Photo-excited electrons travel to the conductive band of the TiO_2 electrode. When the excited state energy level is higher than the lower level of the conduction band, after excitation of the dye molecule, an electron is transported into TiO_2 working electrode and oxidizes because it loses the dye electron. The injected electrons are

spread throughout the metal oxide and move through external the circuit in counter-electrode[24]. The equation for electron injection is shown in (2.2)



2.1.2.3 Dye Regeneration

In order to convert the existing dye from its oxidized state to its original state, it needs to receive electrons in a continuous cycle, which is obtained by using the I / I₃ redox couple in the counter electrode. As the oxidized dye is converted to ground, electrons are taken from iodide ions and then triiodide is oxidized. Electrons injected on the back contact, reducing the oxidized dye by reaction with iodide produces triiodide, to reduce the redox mediator[25]. The equation for dye regeneration is shown in (2.3)



The triiodide ions are then diffused in the counterelectrode where they are reduced to iodide by electrons coming from the external charge. The equation for Tri-iodide reduction is shown in (2.4)



In addition, the triiodide spread around the counterelectrode and replenishes the iodides by accepting electrons from the external load.

2.1.2.4 Recombination Losses

The charge recombination that occurs at interfaces is a factor in DSSCs that gives rise to photogenerated electron losses and negatively affects the performance of DSSCs. There are two energy loss states for the injected photoenergetic electron. The first case comprise converting the electron to the ground state dye (S), which is also referred to as back electron transfer, by recombination with the oxidized sensitiser

(S^+) [26]. The equation for recombination with the oxidized sensitiser is shown in equation (2.5).



The second energy loss state occurs as the consequence of the reaction of the conduction band electrons with the oxidized redox couple on the TiO_2 surface. Normally the reaction must be on the counter electrode, but on the surface of the semiconductor nanoparticles. The equation for recombination on the TiO_2 surface is shown in (2.6).



If A high performance charge transfer is desired, the iodine reduction rate as the counter electrode must be several cycles faster than the recombination at the TiO_2 / electrolyte interface [27]. The working architecture of a DSSC is seen in Figure 2.2.

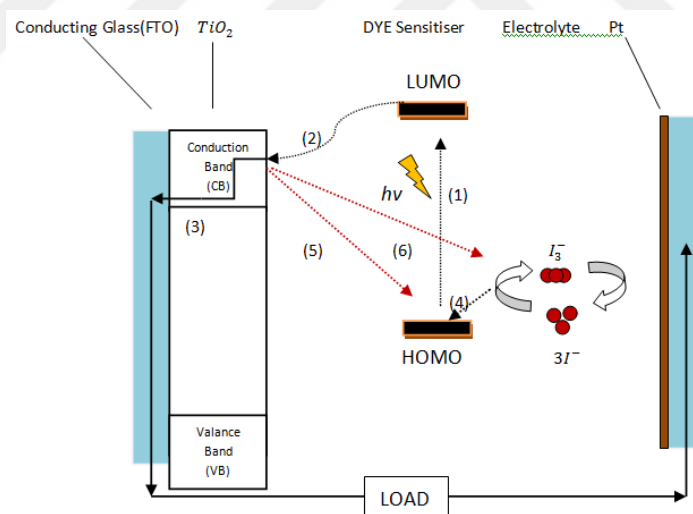


Figure 2. 2 Architecture of working principle and electron conduction steps in a DSSC.

When the incoming light strikes, the dye absorbs a photon and an electron is excited to the LUMO level of the dye molecule (1). The injection of this excited electron is carried out in the semiconductor conduction band(2). The injected electron moves towards the back contact to the external electric circuit by diffusion in the TiO_2 film(3). The dye, which lost electrons, is regenerated by the electron obtained by the reduction of triiodide in the redox electrolyte pair(4). Conduction band electrons in

TiO_2 react with oxidized dye molecules to form recombination(5). recombination possibility of electrons in the conduction band with I^3 in the red-ox(6) [28].

2.1.3 Performance parameters affecting the efficiency of DSSCs

The electricity generation from the photon energy conversion is provided by the photovoltaic device's ability to generate voltage over an external load and also current is obtained over a load [29]. The performance of DSSCs is usually characterized using JV curve parameters. The evaluation parameters resulting from the JV curve are short-circuit current (I_{sc}), open-circuit voltage (V_{oc}), maximum voltage(V_m), maximum current (I_m), fill factor (FF) and efficiency (η).The J - V curve of a DSSC is shown in Figure 2.3 [30].

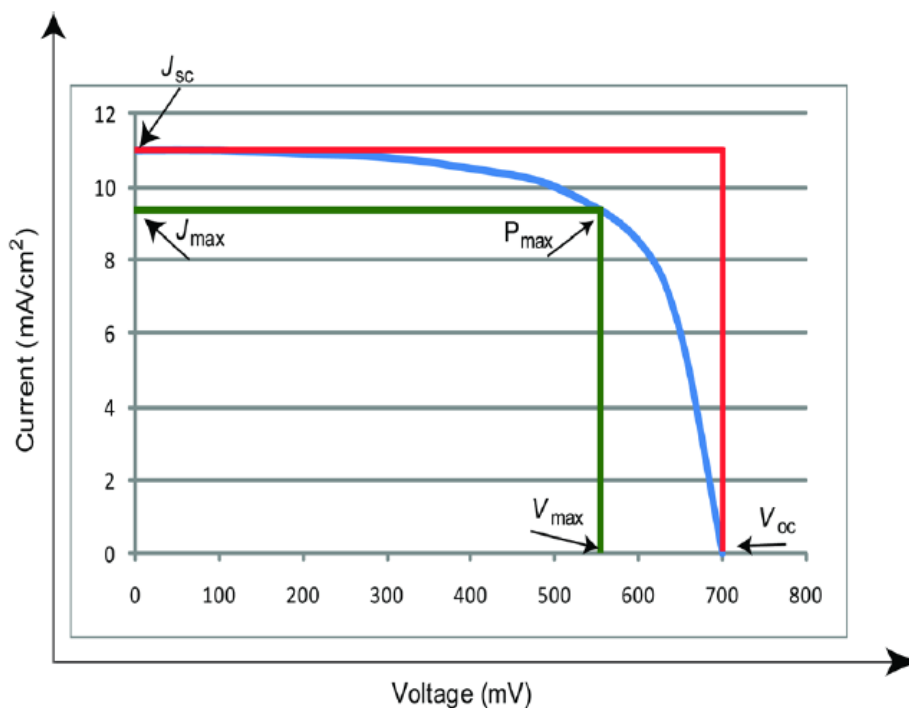


Figure 2. 3 J - V (current density-voltage) curve

2.1.3.1 Short Circuit Current I_{sc}

I_{sc} is the current that flows through the solar cell when the output voltage of the DSSC is zero, that is to say that when no current is resisted by any external resistance. The I_{sc} can be thought of as the maximum current that an ideal

photovoltaic device can produce, until the external load is connected to the circuit. The short-circuit current corresponds to the number of photons converted to hole-electron pairs that result in illumination. The short circuit current varies according to on a series of factors. These are the adsorbed dye molecule, diffusion electrolytes, temperature and dye loading [31]. Conceptually, the short circuit current density (J_{sc}) is defined as the ratio of short circuit photocurrent to the effective area of solar cell. The equation for current density is shown in (2.7).

$$J_{sc} = I_{sc}/A \quad (2.7)$$

2.1.3.2 Open Circuit voltage V_{oc}

If the output current of the solar cell is zero, it is the maximum voltage that can be obtained by an infinitely resistive load that is assumed to be connected to its ends from a solar cell. In other words, V_{oc} is the difference in the electrical potential between the two terminals of an illuminated cell when the circuit is open, ie no current flows. V_{oc} corresponds to the energy difference between the Fermi energy level below the conduction band of TiO_2 , and the redox reduction and oxidation pair within the electrolyte, as shown below [32]. The major factors affecting V_{oc} are recombination occurring in electrolyte, band gap of TiO_2 , redox activity, dye molecule.

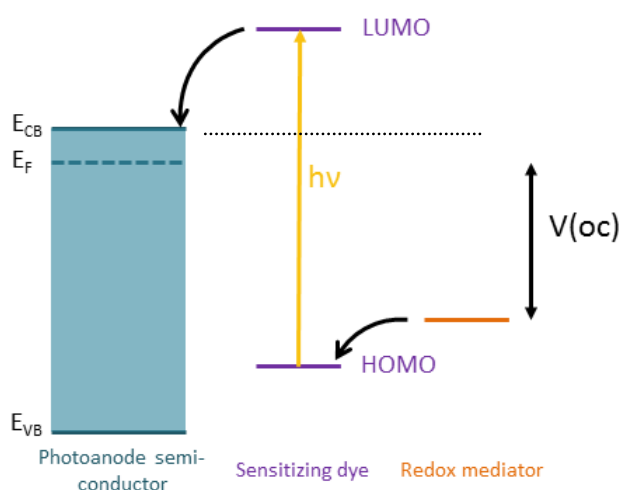


Figure 2. 4 Schematic representation of V_{oc}

2.1.3.3 Maximum Voltage V_m

V_m is the maximum value at the point where the largest rectangle that can be plotted in the area below the JV curve is located at the axis where the voltage is located.

2.1.3.4 Maximum Current I_m

I_m is the maximum value at the point where the largest rectangle that can be plotted in the area below the JV curve is located at the axis where the current density is located.

2.1.3.5 Fill Factor FF

Fill Factor is abbreviated as FF and is a parameter that shows the ratio of the maximum power obtained from the solar cell, which is shown in cut-off points of the plotted largest rectangle below the JV curve, to the power of an ideal solar cell having open-circuit voltage and short-circuit current. FF varies between 0 and 1, with a value of 1 meaning zero internal cell resistance. FF is closely related to the increase and decrease in series and shunt resistance of the solar cell. FF shows the degree of electrical and electrochemical losses in cell operation [33].

To provide a more efficient FF , it is necessary to increase the shunt resistance as much as possible and to reduce the series resistance as much as possible, and to reduce the overvoltage for diffusion and load transfer [34]. The equation for fill factor is shown in (2.8).

$$FF = \frac{I_{max} \times V_{max}}{I_{sc} \times V_{oc}} = \frac{P_{max}}{I_{sc} \times V_{oc}} \quad (2.8)$$

2.1.3.6 Energy Conversion Efficiency η

When formulating the efficiency of the DSSC, the maximum output power (P_{max}) generated by the solar cell is the ratio of the radiation at all wave lengths coming to the surface of the cell. Efficiency is usually expressed as percentages and is the peak at the point where the power given to load, P_m , is the highest. Since the η value is a parameter dependent on V_{oc} , I_{sc} and FF , it is important to keep these parameters at the proper value in order to increase the efficiency, and at the same time the intensity of the incident light and the distribution over all wave lengths is important. By

improving the standard measurement condition, solar cells between different laboratories were more easily comparable. Standard solar illumination is determined by the Air Mass(AM) value. Standard conditions are AM 1.5 at a light power density of $100 \text{ mW} / \text{cm}^2$ and cell temperature of $25 \text{ }^\circ\text{C}$ [35]. The equation for efficiency and maximum power is shown in (2.5)

$$P_{max} = I_{sc} \times V_{oc} \times FF \quad \eta = \frac{P_{max}}{P_{in}} \quad \eta = \frac{I_{sc} \times V_{oc} \times FF}{P_{in}} \quad (2.9)$$

2.1.4 The Basic equivalent circuit of DSSC

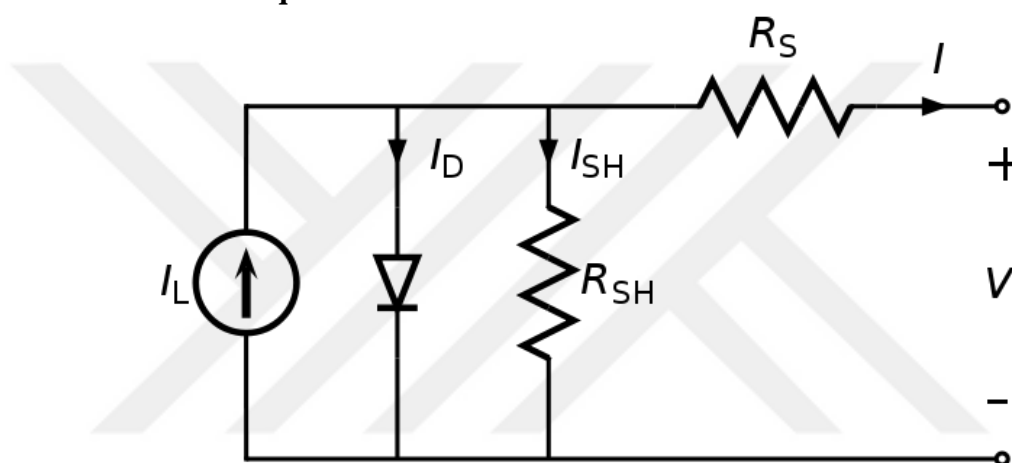


Figure 2. 5 Simple equivalent circuit of DSSC

I = output current

I_L = photogenerated current

I_D = diode current

I_{SH} = shunt current

$$I = I_L - I_D - I_{SH} \quad (2.10)$$

A basic DC equivalent circuit consists of a current source (I_L) in parallel with a series resistor (R_S), a pn junction diode and a shunt resistor (R_{sh}), as seen above figure 2.5 [36]. The current source represents the electron injection obtained from light. R_S is the total ohmic resistance of the solar cell consisting of the electrical resistance of all the materials (film resistance, electrode resistance, and the contact between the film and the electrode.) used in the cell and the interfaces between them. R_{sh} is associated

with loss of carrier recombination at the junction near the cell edges, in relation to the leakage of the current, particularly to manufacturing defects. As the value of the shunt resistor decreases, it provides a split current path for the photogenerated current which leads to significant power loss. In an ideal solar cell, R_s ohmic resistance is zero, while R_{sh} shunt resistance should approach infinity[37]. The equation for output current is shown in (2.10).

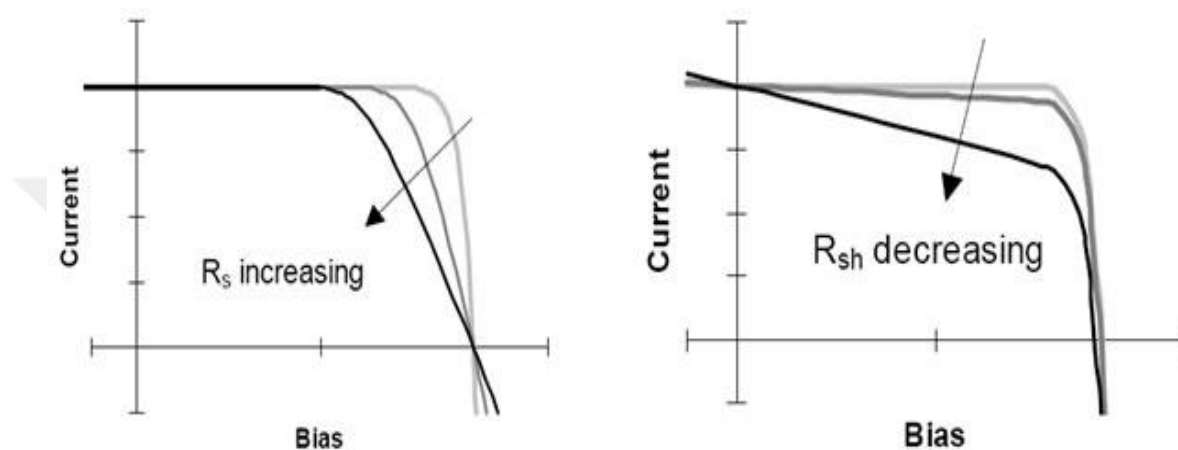


Figure 2. 6 Effect of R_s (series resistor) and R_{sh} (shunt)

As the R_s value increases from zero to infinity, the solar cell exhibits ohmic behavior. As the R_{sh} value decreases towards zero from infinity, the solar cell shows ohmic behavior as well. As the series resistance increases, the short circuit current density decreases and accordingly the FF ratio decreases, as above figure 2.6 [38]. If there is a decrease in the shunt resistance, it negatively impacts the open circuit voltage and causes the proportional decrease in FF . It can be said that the V_{oc} is not affected by R_s since the current through R_s is zero. Although I_{sc} is not much affected by R_s , the resistance at very large values may then cause the I_{sc} to decrease.

The total current in J_{sc} is not affected as long as the short-circuit voltage is not too low, as the shunt resistance is low for the current along the outer path[39]. Very high R_s values cause a significant decrease in I_{sc} , in which the series resistance is overwhelmed and the behavior of the solar cell is like a resistance behavior. The decreasing R_{sh} values will result in a significant reduction in V_{oc} . Like a high series resistance, a poorly shunted solar cell will have similar working characteristics with a resistance. [40].

2.1.5 Literature Review

In 1767 Swiss scientist Horace de Saussure produced the world's first solar collector to build thermal traps [41].

In 1887, the Heinrich Hertz found that the photoelectric effect of electrons spread from the solids, liquids or gases through the energy absorption of light [42].

In 1905, Albert Einstein published an article describing photoelectric effect, presuming that light energy was carried by a quantum energy package which is tiny packets of energy called photons [43] .

In 1932, Audobert and Stora discovered the PV effect of cadmium sulphide (CdS), which is now used in solar cells [43].

In 1954, the current development of solar cell began at the Bell Laboratories Daryl M. Chapin and his colleague produced a silicon-containing cell with 6% [44].

In 1970, the Soviet physicist Zhores Alferov designed a gallium arsenide-based heterojunction solar cells..this was the first solar cell built on the semiconductor materials of group III-V [45].

In the 1970s, photovoltaic technology increased public interest because of the oil crisis that led to a dramatic rise in oil prices. Oil prices continued to increase exponentially for several years as some countries stopped selling oil. This was an important influence on how scientists set out to explore ways to improve solar energy technology, such as PV cells [46] .

In 1980, the first thin film solar cells were produced at Delaware University with a conversion efficiency of about 10% thanks to the copper-sulfur / cadmium-sulfur compound[36]. In 1985, the New South Wales University in Australia made crystalline silicon solar cells with an efficiency of over 20% [45].

In 1991, the first high-efficiency Dye sensitized solar cells which had an improved conversion efficiency of 7.12%, was published by the Swiss scientist Michael Grätzel and his colleagues [7].

In 1998, H. Honda and his colleague point out that the photocatalytic reactions originating from TiO_2 developed illumination irradiation on semiconductors [47].

In 2000, Anders Hagfeldt and Michael Grätzel Under AM 1.5 solar radiation, they succeeded in bringing the overall power conversion efficiency of the new solar cell to 10.4% [48].

In 2006, Kun-Mu Lee and his colleague investigated the effect of surface morphology on the performance of dye-sensitized solar cells with the thickness of the TiO_2 coating cycle and achieved 9.04% efficiency. [49].

In 2009, Ito, Nazeeruddin and Zakeeruddin analyzed the dye sensitized solar cells by adjusting the thickness optimization and observed with the scanning electron micrograph of TiO_2 electrodes and obtain [50].

In 2012, Mounir Alhamed and his colleague achieved a 3.04% efficiency from the dye-sensitized solar cell they prepared as a photosensitizer (1: 1: 1) using a combination of all natural 3 dyes (Rattan, Hibiscus, chlorophyll) [51].

In 2015 Kenji Kakiage and his colleague produced a with efficiency of about 12.8% conversion efficiency by coating with organic silyl anchor dyes [52].

In 2015 Kenji Kakiage and his colleague succeeded in obtaining a record with the highest efficiency of 14.3%, with DSSC having a common sensitization with Silyl-anchor and carboxy-anchor dye [53].

CHAPTER 3

FABRICATION AND CHARACTERIZATION DEVICES

TiO₂ thin films were prepared on FTO coated glass substrates using spin coating technique. The thickness of films was controlled by adjusting the coating cycles (x5, x10 and x15). The crystal structure, optical transmittance and surface morphology of TiO₂/FTO structures were measured by means of XRD and UV-vis spectroscopy, and AFM, respectively. Dye-loading using black mulberry (*Morusnigra*), madder (*Rubiainctorum*) fruits, and eosin y ($C_{20}H_8Br_4O_5$) was applied for 18h. Photovoltaic performance of the solar cells in terms of thickness and dye types was tested under standard conditions.

3.1 Cutting, cleaning and measuring the TCO

To produce DSSC, first a substrate is required, which is a glass plate coated on one side with a Transparent and Conductive Oxide (TCO) layer and on the other side with an insulating coating. In general, indium tin oxide (ITO) or fluorine doped tin oxide (FTO) is used while DSSC is being produced. In this study, FTO was preferred as substrate. The FTO glass was cut into 3 pieces 2.5 cm X 2.5 cm X 0.3 cm dimensions using a glass cutter. These FTO substrates should be cleaned in order to eliminate any contaminants that will affect conductivity on the surface, transparency, surface morphology which makes it easier to stick the subsequent layers to contribute to the sandwich structure at the end of the cleaning process.

- First, the surfaces of the FTO coated glass were cleaned with sponge softly so as not to be scratched.
- Ultrasonic cleaner bath (as shown fig 3.1) in detergent solution for 15 min
- Rinse with deionized water
- Ultrasonic cleaner bath in acetone for 15 min
- Ultrasonic cleaner bath deionized water for 10 min
- Ultrasonic cleaner bath ethanol for 10 min
- Ultrasonic cleaner bath deionized water for 10 min

- TCO films were air-dried by 4 bar of air



Figure 3. 1 Ultrasonic cleaner bath used in measurement

To determine which side of the TCO is conductive, a certain resistance value about ($\sim 10 \Omega/\text{sq}$) is read by contacting the two conductive sides of the multimeter probes. In order to get a contact from the conductive part of the TCO, it was used until the end of the deposition process so as not to lose the conductivity of the FTO with an insulator of about 0.5 cm before the coating started.

3.2 Preparation of solution and deposition of TiO_2 on TCO

Titanium(IV) isopropoxide (TTIP), triethylamine (TEA) and acetic acid (HAc) were purchased from Sigma-Aldrich Co. 5.116 g of TTIP (0.6 M), 1.821 g of TEA (0.6 M), 1.081 g of HAc (0.6M) (1: 1: 1: 30 ml) in separate flasks and in each 10 ml of ethanol at a rotation speed of 400 rpm were stirred at room temperature for 15 minutes. The solutions dissolved in 10 ml of ethanol in separate flasks were mixed in a single flask after stirring for 15 minutes at room temperatures. The resulting mixed solution was stirred using magnetic stirrer bar at 50°C for 2 hours at a rotation speed of 400 rpm. The prepared mixture was subjected to aging in sterile environment at room temperature for about 24 hours so as to reach a gel consistency. The TiO_2 mixture was prepared by the sol-gel method as shown figure 3.2.

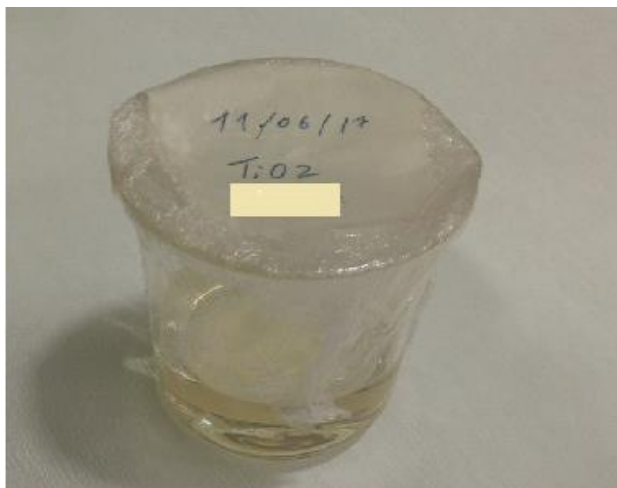


Figure 3. 2 TiO₂ prepared by the sol-gel method

After 24 hours of aging, the mixture was ready to be coated on TCO. After 24 hours of aging, the mixture was ready to be coated on TCO. Before the solution was dropped onto the FTO coated glass, the conductive side was identified and the conductive side was sealed with tape to allow one side to be used as a contact in the future. For each coating cycle, 50 μ l of the mixture were taken with the aid of adjustable tip ejector and was dropped on the FTO glass placed on the spin coater device (shown as Figure 3.3).



Figure 3. 3 Spin coater device

FTO glass with TiO₂ drop on it rotates for 30 seconds at 0 acceleration time at the spin rate of 2000 rpm in the spin coater device. FTO glass taken out of the spin coater was preheated at 500 °C for 5 minutes to deposit TiO₂ particles uniformly on

the FTO surface using a programmable OptoSense brand tube furnace (seen as figure 3.4). After the TiO₂ coated FTO glass from the furnace was cooled outside for 5 minutes, the first cycle was completed using spin-coating method.



Figure 3. 4 OptoSense tube furnace used for annealing

Depending on the number of coatings cycles, this process was repeated 5, 10 and 15 cycles, respectively. After each sample had its own number of coating cycles, it was annealed at 500 °C for 1 hour in the same furnace.

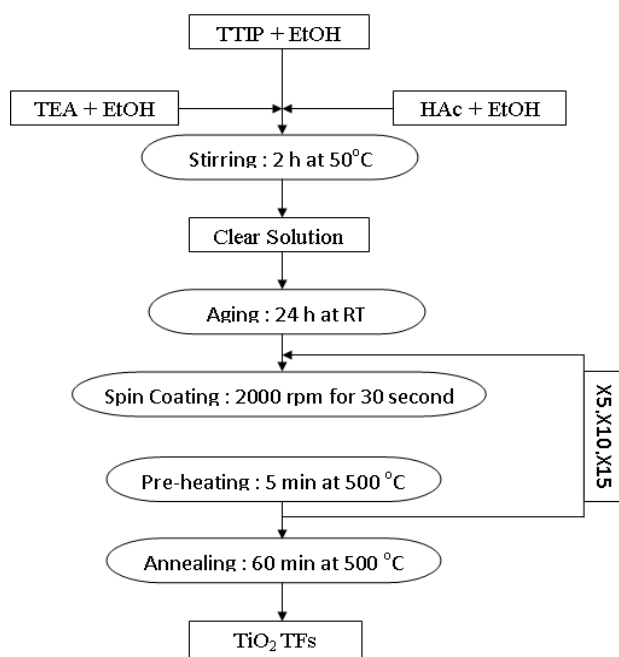


Figure 3. 5 Coating cycle steps of TiO₂ thin films

3.3 Dye Sensitiser Extraction and Preparation

Since titanium dioxide is a semiconductor with white color, it does not have the ability to absorb light at visible wavelengths alone too much. For this reason, the dyeing process is important to color and sensitize the titanium electrode and to increase the absorption of the light in the visible light spectrum. The dyes used in the dyeing process were black mulberry (*Morus nigra*) (30 g: 0 mL), madder (*Rubiatinctorum*) (30 g: 10 mL), and eosin y ($C_{20}H_{8}Br_4O_5$) (3 mM: 10 mL). Eosin Yellowish was purchased from Carlo Erba Reagents and dissolved in 10 ml Ethanol. Madder was gathered from the nature and boiled for 2 hours in water so that its roots would be vertical. As boiling continued, a certain amount of NaCl was added to allow for better extraction of the dye. Then, the solid particles were then filtered to extract the dye as a liquid. Black Mulberry was crushed until water was obtained and filtered using a paper filter to get the liquid from the solid particles.



Figure 3. 6 Preparation process of dyes

Black Mulberry was crashed until it became liquid. After crushing, the solid particles were filtered using a paper filter to get the liquid. The process of preparing the dye is shown in figure 3.6.

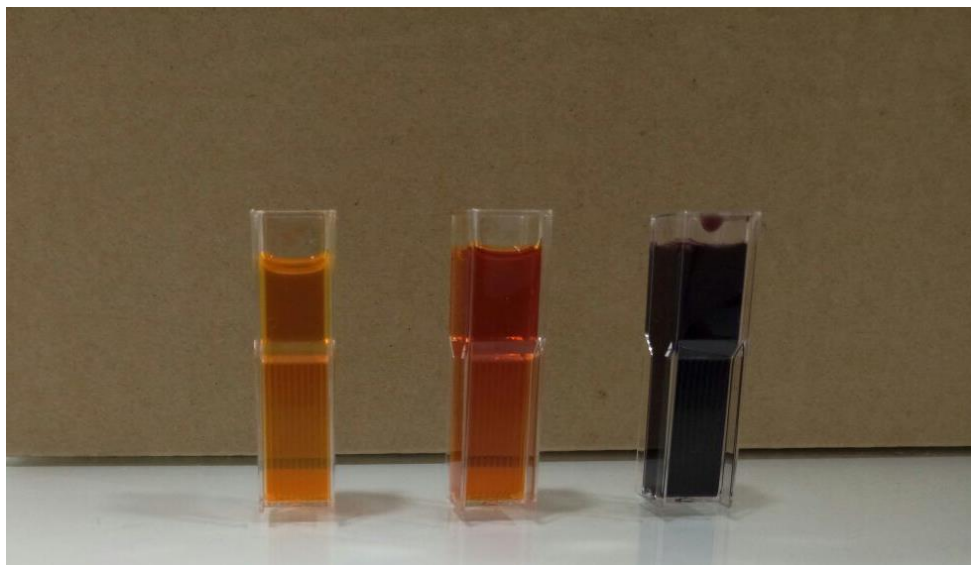


Figure 3. 7 The dyes extracted

After obtaining the dye extracts (as shown figure 3.7) , the TiO₂ thin films produced in the previous step were left in the dye extracts for 24 hours to perform a molecular bond with the dye in petries and petries were labeled (as seen figure 3.8). Finally the thin films washed in ethanol to remove any contaminants.

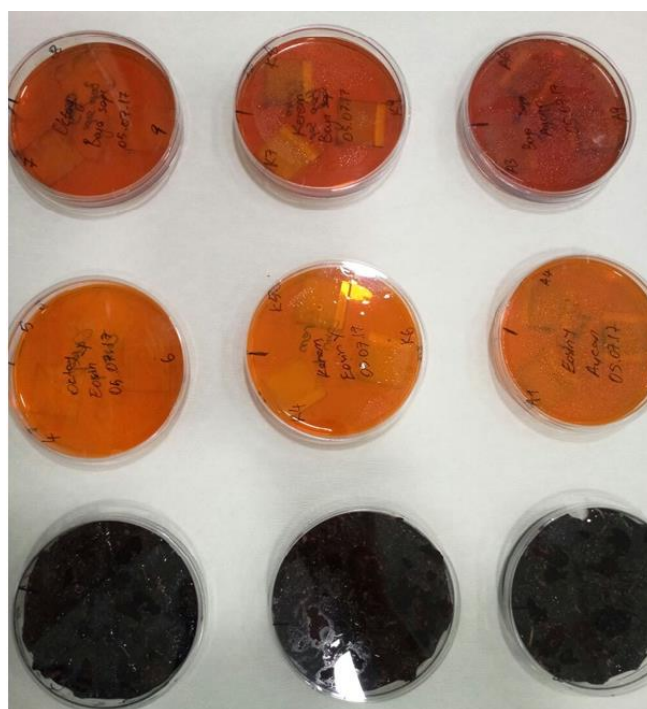


Figure 3. 8 Dyeing of TiO₂ in petryls

3.4 Preparation of electrolyte

Electrolyte is an important process for improving the efficiency of DSSC because it contains redox couple reactions (reduction and oxidation), and these reactions contribute to the re-production of the dye by giving electrons to the oxidized dye. The iodide / tri-iodide electrolyte solution containing the redox couple in which the reduction-oxidation reactions are carried out was prepared using 0,05 M iyot (I_2) ($\geq 99.8\%$, Sigma-Aldrich), 0,5 M lityum iyodür (LiI) ($\geq 98.0\%$, Merck), and asetonitril (99.9 %, Sigma-Aldrich). Iodine and Lithium iodide were separately mixed in acetonitrile, dissolved and then combined to prepare a liquid ionic electrolyte solution.

3.5 Preparation of Counter Electrode

The contribution of the counterelectrode to the DSSC is to terminate the circuit with the working electrode and the electrolyte. The triiodide is also reduced to the iodide for electrolyte regeneration, so that the counter electrode surface should be operated with the appropriate catalyst such as Pt in electron transfer. Cleaning, cutting and taping process of FTO coated conductive glasses used in making thin film was also done in counter electrode. Platisol T/SP (Solaronix, Switzerland) with ethanol for 15 minutes at 500 rpm in a magnetic stirrer were stirred and the solution was prepared. 100 μ L Platisol solution in each cycle was dropped onto FTO glass. Using the spin-coating method, the coating parameters were set at a rotation speed of 2000 rpm at 0 acceleration time, for 30 seconds. After the completed coating process, firstly It was heated 80 °C on a hot plate, finally annealed on tube furnace at 450 °C for 30 minutes on air ambient.

3.6 DSSC Fabrication

The complete assembly of the film consists of a TiO_2 working electrode coated with a dye and a FTO substrate counterelectrode coated with a Platisol T/P solution. To form the DSSC sandwich structure, the liquid electrolyte solution of the redox reactions is poured between the previously produced TiO_2 and the dye-coated

working electrode and the Pt-coated counter electrode. The fabricated DSSC structure was attached with two latches (as seen figure 3.9).

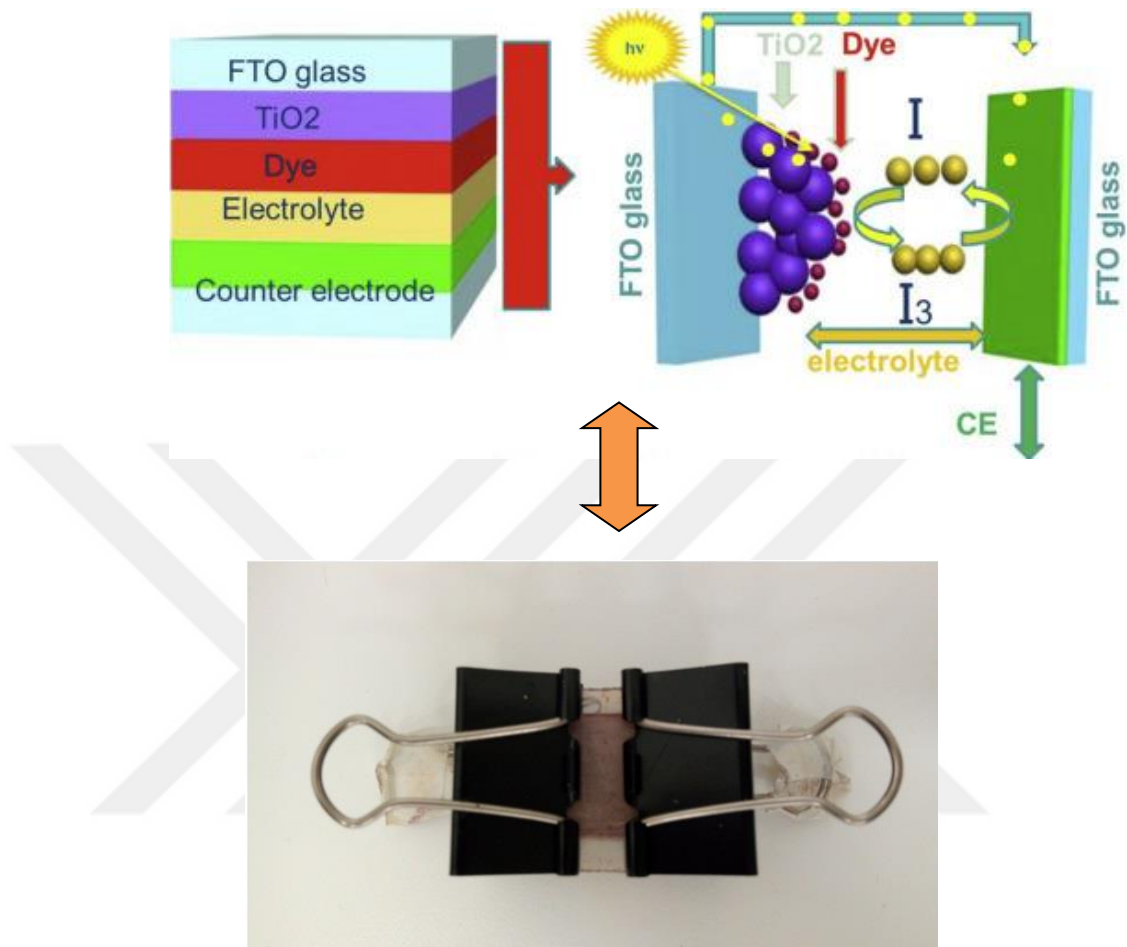


Figure 3. 9 Fabrication of dye sensitized solar cell

3.7 Characterization Methods Devices Of DSSCs

3.7.1 X-ray Diffraction (XRD)

The most commonly used diffraction technique for studying crystal structures of the solids is X-ray diffraction. XRD is based on the principle of diffraction X-rays in a characteristic order, depending on the specific atomic sequences of each crystal phase. For each crystal phase, these diffraction profiles define that crystal as a kind of fingerprint. This technique is suitable for thin film analysis, mainly due to two reasons; 1. The wave lengths of X-rays are measured at the atomic distances in the condensed material, and this property allows them to be used in structural

investigations. 2. X-ray diffraction techniques are not destructive and do not alter the sample being examined[54]. When X-rays are incident on the crystal structure, the rays propagate from the solid surface through the small incidence angles with full reflection, and the rays are scattered by the parallel planes of the atoms in the crystal. The diffraction of X-rays in the crystal structure is explained by the Bragg Law and the Bragg law is given by the following formula in its simplest form[55]. Bragg's law diagram is shown figure 3.10 below [56]. The equation for Bragg's law is shown in (2.11).

$$n \cdot \lambda = 2d \sin\theta \quad (2.11)$$

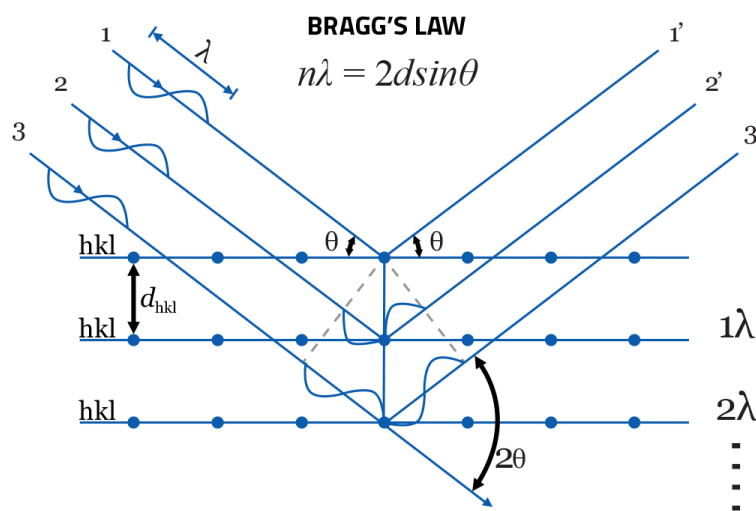


Figure 3. 10 Bragg's law diagram

n = Wave length number

λ = the wavelength of the incident X-rays

d = distance between planes in the atomic lattice

θ = angle of the incident beam with the plate

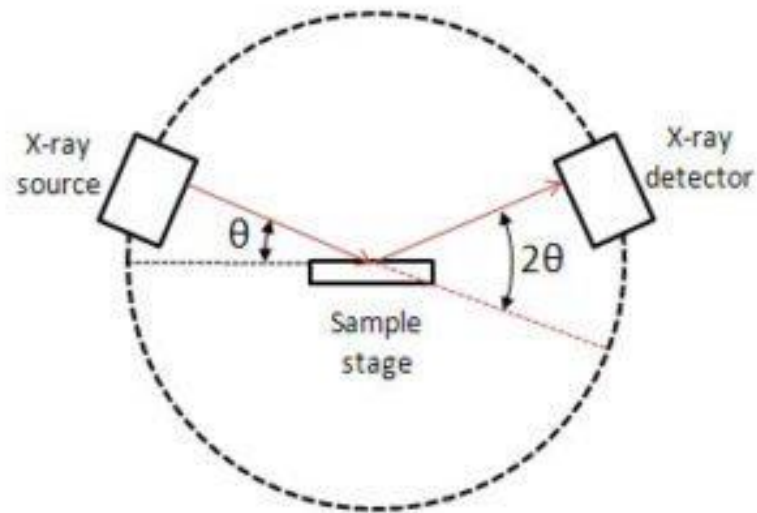


Figure 3. 11 Working Principle of X-ray Diffraction (XRD)

The source emits X-rays that hitting the crystal at a certain θ angle, and the detector scans the scattered radiation at 2θ from the source. Working principle diagram of XRD is shown figure 3.11 above [57]. X-rays strike the atoms in the crystal plane and the rays are scattered in different direction. To be able to diffraction, it depends on the scattered radiation must be consistent, so the scattering being flexible.



Figure 3. 12 XRD used in measurements

The angular position of the source varies in the relevant range and accordingly in the detector, and the intensities of the diffuse rays are recorded and marked according to 2θ . There can be several types of detectors. An XRD pattern is obtained with this plot of 2θ of the intensity of the scattered radiation. The point at which the peak density is maximum is adjusted according to a scale of 100 and the rest of the peaks are scaled accordingly. The resulting peak values are matched to a given group of lattice planes given by the associated miller indices [57]. Measurements were performed using a Rigaku Miniflex 600 XRD instrument (as shown figure 3.12). Considering the places where the diffraction peaked, the phases of the sample, the amount of phases, crystal size, lattice parameters, changes in structure, crystal orientation and atomic positions can be revealed.

3.7.2 Atomic Force Microscope (AFM)

Atomic force microscopy is a recent imaging technique used for surface imaging and surface imaging at the molecular level. AFM is a microscope capable of displaying surface topography up to 100 microns (μ) from the angstrom (\AA) range [5].

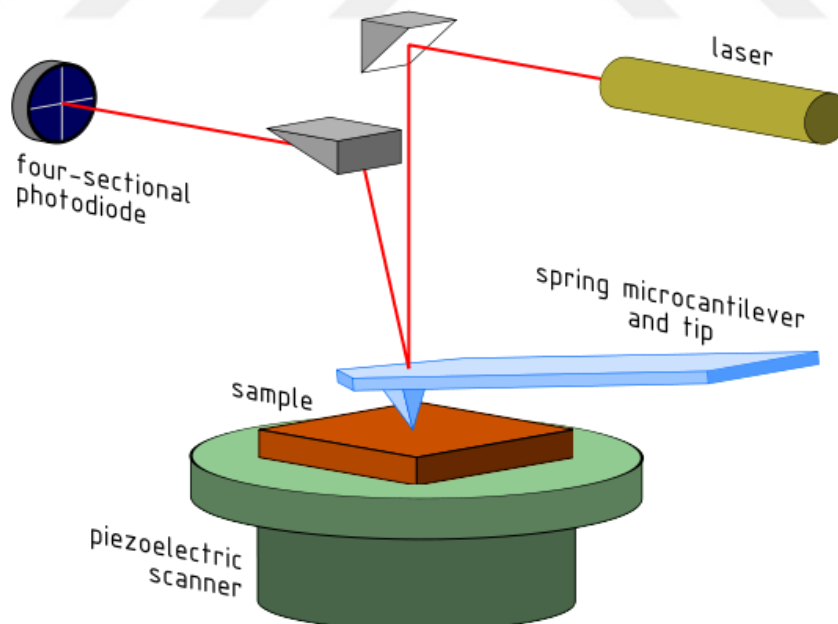


Figure 3. 13 Working principle of AFM

AFM is used in topological analysis of the surface properties of thin film coatings of conductive glasses coated with FTO and then coated with TiO_2 for use in DSSC

sandwich construction. The AFM uses a rod called a cantilever to scan the surface of the sample and a very thin needle at its end. When this needle comes close enough to the surface, it causes the gravitational forces between the surface and this needle to deviate towards the surface of the cantilever. As the needle gets closer to the surface, as it touches the surface, the pushing force increases and the cantilever deviates from the surface. Working principle of AFM is shown figure 3.13 above [58]. The needle used at the end varies according to the surface to be examined. With the help of a laser beam, cantilever deviations towards the surface or away from the surface are detected. The laser beam is reflected through the cantilever material. As the cantilever moves, the angle of the reflected beam also changes. Position sensitive photo diode (PSPD) is also used to detect these changes [59]. With these deviations in the laser beam, surfacerecess and protrusions in the examined nano-scale are recorded. By analyzing the deviations from the laser beam, the position information on the surface is also recorded. The analysis results are similar to embossed maps. Just as in embossed maps, the mapping of the examined nano-surface is made to the differences in the height of the corresponding position. Thus, a topographic image of the nano-surface is obtained[60]. AFM used in measurements is seen figure 3.14.

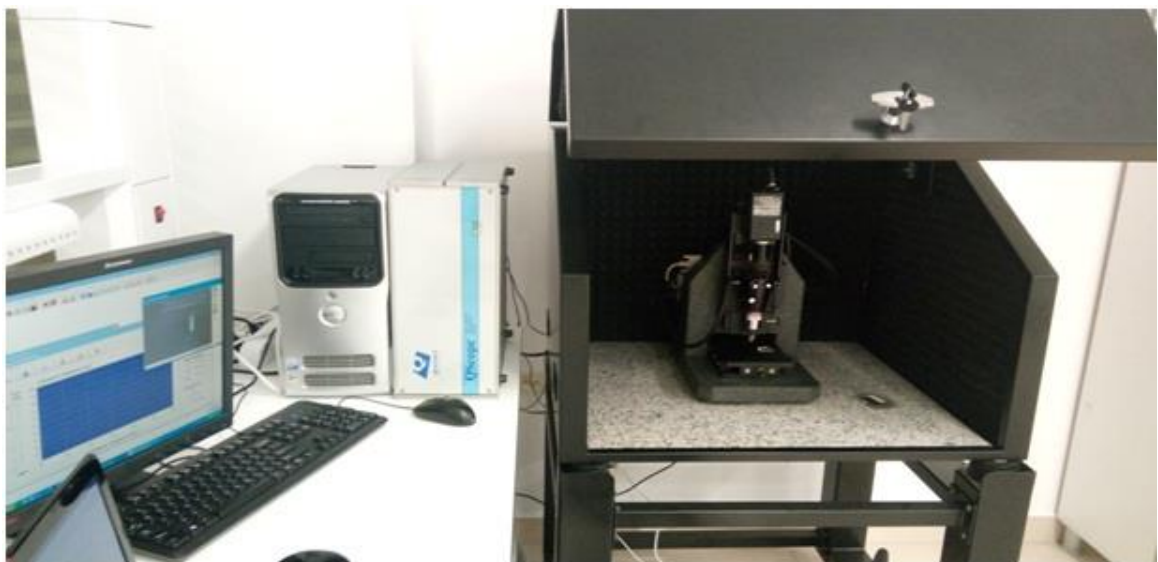


Figure 3. 14 AFM used in measurements

3.7.3 UV-Vis Spectroscopy

Ultraviolet and visible light (UV-Vis) absorption spectroscopy is used to determine how much of a beam applied to a solar cell is absorbed after passing through a solar cell, and how much is reflected back. Working principle of UV-Vis is shown in figure 3.15 [61]. A decrease in the intensity of the light indicates an increase in absorption. The atoms or molecules of the material to be examined in the emission spectroscopy are stimulated as a result of applied external influences and emit photons. Since the atoms or molecules that make up the material have their own arousal levels, the material studied can only emit photons at certain energies. These photons sent are analyzed by spectrophotometer and it is possible that we have information about the material. In the absorption spectroscopy, the electromagnetic wave is sent on the material to be investigated, and the photons, which are in order to stimulate the atoms or molecules in the energy material, are absorbed with certain possibilities[61].

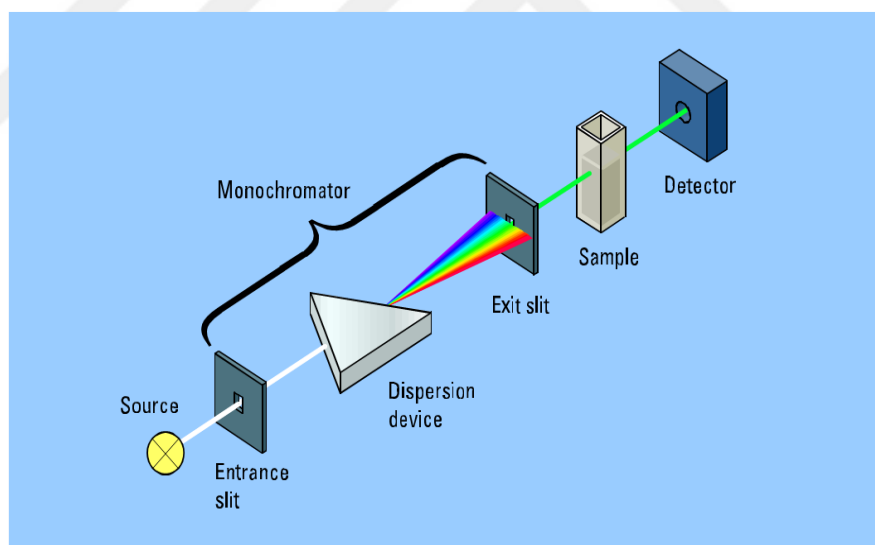


Figure 3. 15 Working principle of UV-Vis

When the electromagnetic waves passing through the material are analyzed, the count value is reduced or the dark areas are formed at the wavelengths corresponding to the absorbed photons. The wavelengths at which these count values are decreasing or dark regions are different for each atom or molecule. Therefore, the values

obtained as the result of analysis provide us with information about the material. [62]. After exiting the light source, the light passing through the sample and reaching the photodetector is compared with the light sent from the spectrophotometer and the absorption, transmittance graphs are obtained. Measurements have been performed using the Shimadzu Corporation UV-1700 series (as shown figure 3.16).



Figure 3. 16 UV-Vis used in measurements

3.7.4 Solar Simulator

Solar simulators are used to determine the characteristics of short circuit current density (J_{sc}) and open circuit voltage (V_{oc}) parameters by artificial light under the AM 1.5 G $100 \text{ mW} / \text{cm}^2$ standard illumination of the manufactured solar cells. With the illumination of the Xe arc lamp contained in an elliptical reflector, the collected light spectrum is reflected via a mirror and after passing through the AM 1.5 G filter and homogenizer, the light is again reflected by another mirror at a certain angle, and the condenser filter allows the light to focus on the sample. Figure 3.17 shows the working structure [63].

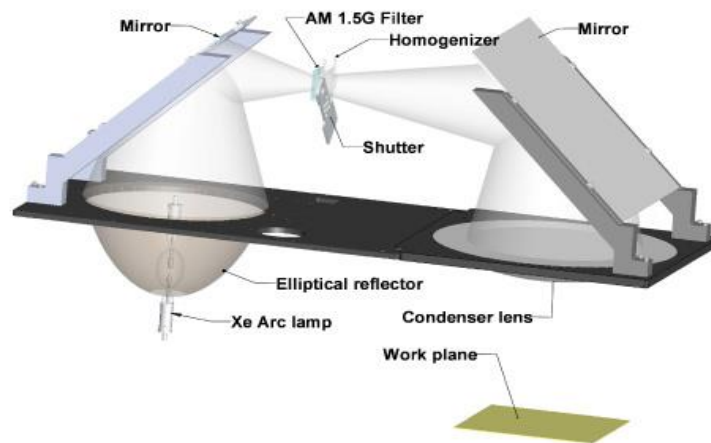


Figure 3. 17 Solar simulator working mechanizm

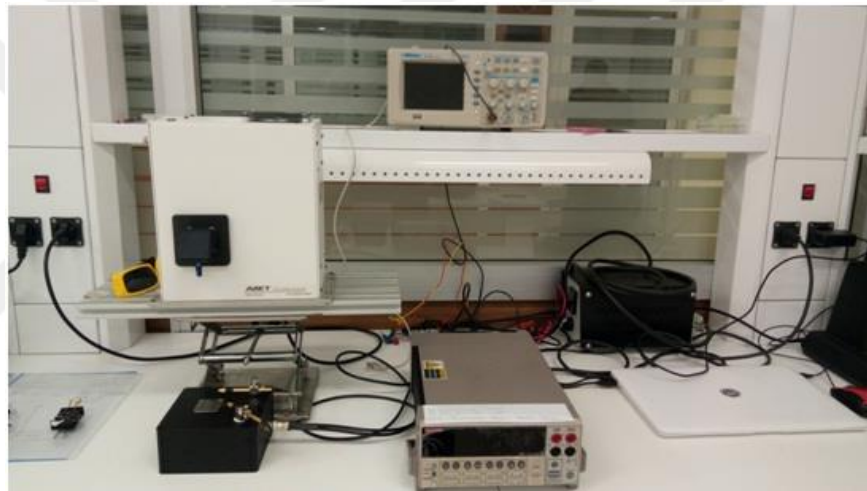


Figure 3. 18 Solar Simulator and sourcemeter used in measurements

As a solar simulator, Abet Technologies device was used (as shown figure 3.18). Analysis of the electrical values produced in the DSSC by means of the incident light on the sample due to artificial solar irradiation was obtained using a Keithley 2400 source meter.

CHAPTER 4

RESULTS

The crystallinity of the annealed film was examined by X-ray diffraction (MiniFlex 600, Rigaku Co., Japan) using Cu K α radiation at $\lambda=0.1546$ nm, in the range of 2θ , 20–60°. Absorbance in the visible wavelength range was observed by using a UV–visible–NIR spectrophotometer (UV-1700 Spectrophotometer, Shimadzu, Japan). Atomic force microscopic (AFM) images of the surface in a $40\mu\text{m} \times 40\mu\text{m}$ area were achieved to be used an AFM (Q-Scope 250, Quesant Instrument Corporation, USA). A device area of 1 cm^2 was defined by *3M rubber adhesive vinyl waterproof tape*. Masked devices were tested under a solar simulator (Abet LS 150, Abet Technologies, Inc., USA) at AM1.5 and 100 mW/cm^2 illumination conditions calibrated with a *SRC-2020 Solar Reference Cell*.

4.1 Structural Results

XRD measurements were made to examine the crystal structures and orientations of each of the 5, 10, 15 cycles TiO₂ coated samples.

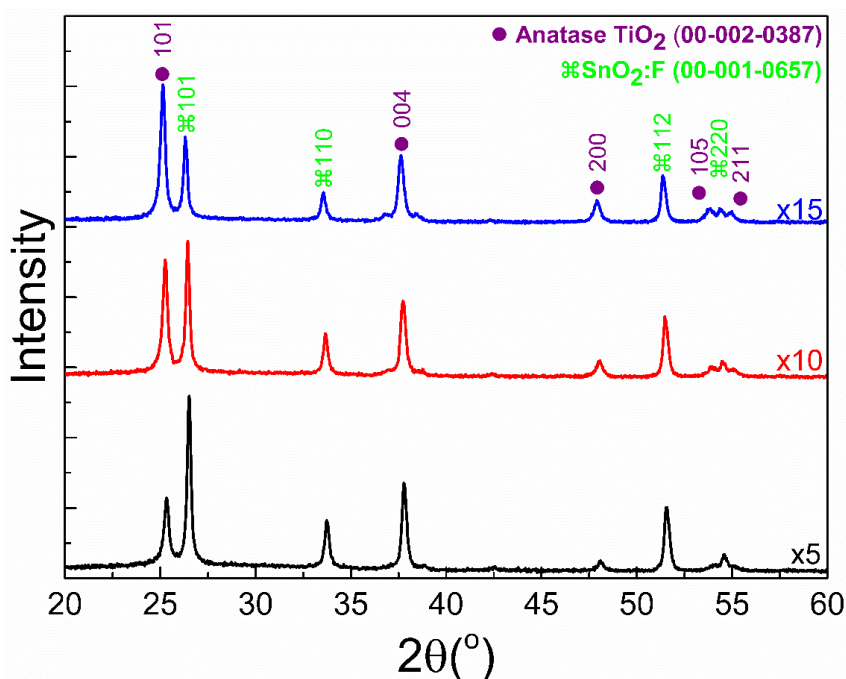


Figure 4. 1 XRD spectra of TiO₂ samples coated on FTO glasses.

Figure 4.1 shows XRD spectra of TiO_2 samples. The peaks of the anatase phase of TiO_2 and their orientations are also marked by considering JSPDS cards. From the XRD results, anatase (101), phase peak and orientations specific to TiO_2 were observed in the structure. The phase structure of the samples is a tetragonal crystal anatase and has a preferred orientation of (101). When the intensity and full width half at maximum values for (101) orientation, better crystal structure is obtained as the coating cycle increases. This improvement can be due to an increase in the film thickness. There is a trend in favor of crystal quality with increasing the film thickness. In addition, Once analyzed the crystal structure of the samples , peaks arising from FTO were also observed. It was seen that these peaks were at the same level in all the samples.

4.2 Morphological Results

Figure 4.2, Figure 4.3 and Figure 4.4 depicts AFM results of the samples 5, 10 and 15 cycles coating cycles, respectively. The surface properties and roughness(RMS) values were determined by using these measurements. Properties were affected from the coating cycle. RMS values were estimated to be 606, 466, and 682 nm for 5, 10 and 15 cycles coating cycles, respectively. Generally high RMS value is desired to have high surface area which turns out high absorption of incident light on to solar cell. Therefore, these results indicate that the sample with 15 cycles coating cycle seems to be the best in terms of solar cell among others.

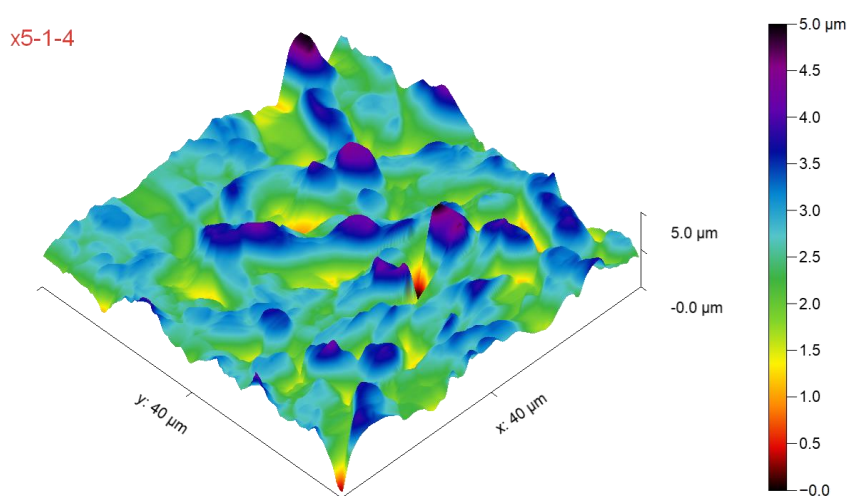


Figure 4. 2 Surface morphology of TiO_2 5 cycles Working electrodes

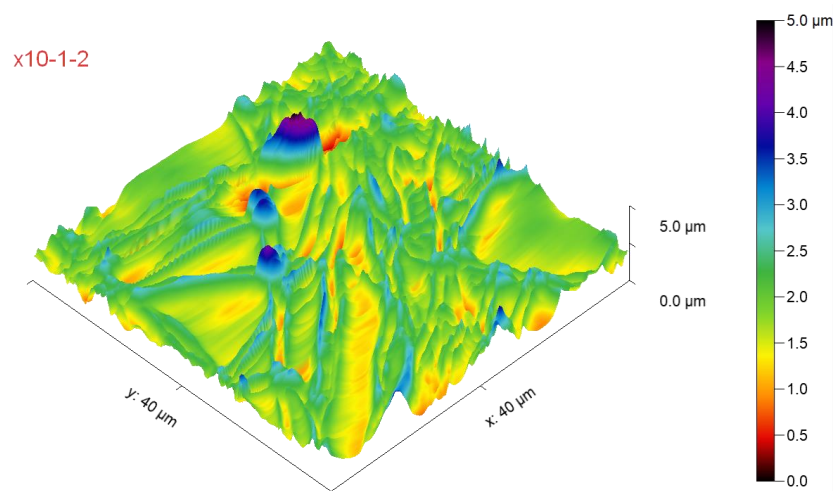


Figure 4. 3 Surface morphology of TiO₂ 10 cycles Working electrodes

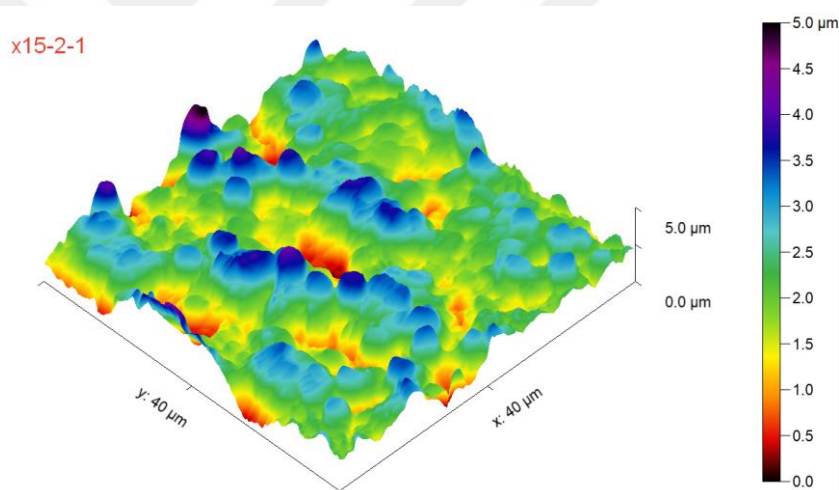


Figure 4. 4 Surface morphology of TiO₂ 15 cycles Working electrodes

4.3 Optical Results

The optical absorption of the films were measured by the UV-Vis Spectrophotometer (UV-1700 Spectrophotometer, Shimadzu, Japan). Coated 5, 10, and 15 cycles with dye-loaded TiO₂ were observed in the spectra of the 400-700 nm wavelength. Before the dye was loaded, the intensity of the absorbance increased as the coating cycle increased. This is an expected result. Since increasing the coating cycle leads to an increase in the thickness of the samples. Thicker film means higher absorption.

Despite being used in the same amount, it is obvious that the different types of dyes have different absorption effects on the same thickness and therefore different spectra. This shows that each dye's ability to absorb light is different from each other. The application of dyes in all its spectra has improved the light absorption. The best result for all thickness values was found with black mulberry and then madder. Eosin yellowish is behind organic dyes. It has been observed that the increase in the absorbance increases the value of the thickness. This trend has also been observed in dye absorption.

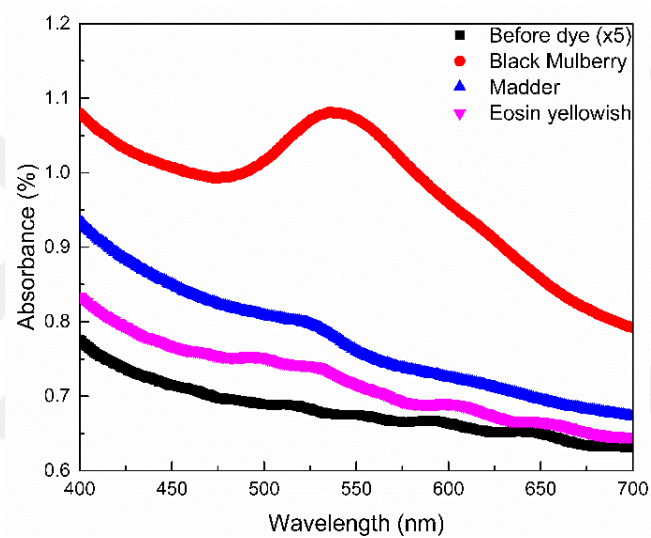


Figure 4. 5 Absorbance spectra before and after dye loading of TiO_2 with 5 coating cycles

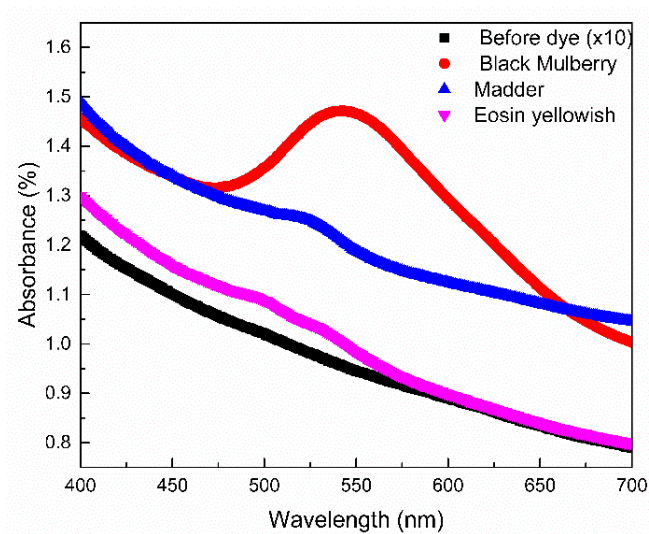


Figure 4. 6 Absorbance spectra before and after dye loading of TiO_2 with 10 coating cycles

The highest absorption value belongs to the sample with 15 coating cycles which is later loaded with black mulberry. After dye loading, new peaks of absorbance at long wavelengths occur. A significant peak was noticed at about 550 nm with black mulberry. This demonstrates that this dye matches well with the peak observed with Ru. Therefore, it might be a candidate for solar cell applications.

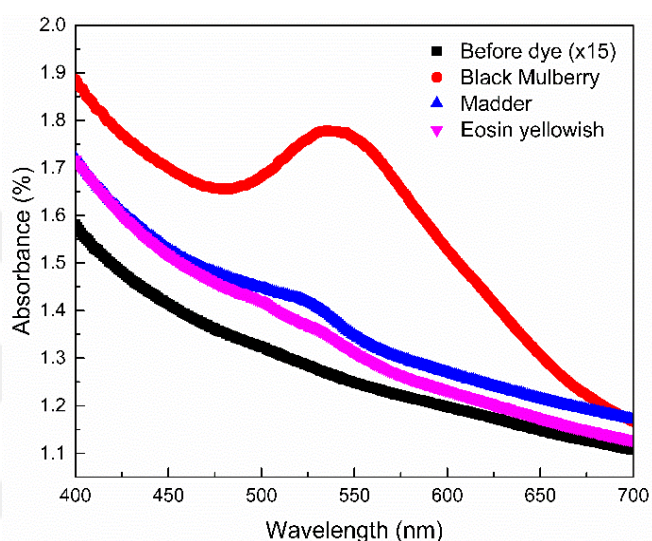


Figure 4. 7 Absorbance spectra before and after dye loading of TiO_2 with 15 coating cycles

4.4 Electrical Results

In order to analyze the photovoltaic performance of the DSSCs, photocurrent density - voltage ($J - V$) characteristics of DSSCs cells were measured with a Keithley 2400 source meter under the artificial solar simulator device set under standard conditions AM 1.5 at a light power of $100 \text{ mW} / \text{cm}^2$. Photovoltaic behavior of 5, 10, 15 cycles coated TiO_2 was observed by using different dyes. Using Eosin yellowish and Madder dyes, the J_{sc} value increased as the number of coatings increased, but the J_{sc} value peaked in the 5 cycles black Mulberry sample, the value dropped almost halfway in the 10 cycles coated sample, then rose again in the coated sample 15 cycles. The current density value was highest in the sensitized structure with Black Mulberry dye coated with 5 cycles TiO_2 . Looking at the V_{oc} values, there was a

progressively increase in the open circuit voltage, regardless of the effect of different dye types, with the increase in thickness. The highest V_{oc} value was attained in a solar cell sensitized with 15 cycles coated TiO_2 with loading of Madder dye.

Table 1 The photovoltaic parameters of DSSC obtained with different coating cycles and dyes of TiO_2

Coating circle	Applied dye	Jsc (mA/cm ²)	Voc (mV)	FF (%)	Rsh (Ω)	Rs (Ω)	η (%)
x5	Black Mulberry	10.67*	329.77	22.30	26.36	39.96	0.78
	Madder	2.68	273.64	28.40	135.45	74.97	0.21
	Eosin yellowish	3.78	365.70	37.50	301.10	24.59	0.52
x10	Black Mulberry	5.69	392.36	41.80*	258.18*	14.06*	0.93
	Madder	3.42	303.62	28.50	131.60	39.16	0.30
	Eosin yellowish	5.58	410.17	38.80	224.68	17.95	0.90
x15	Black Mulberry	9.08	416.13	34.50	97.67	15.60	1.30*
	Madder	7.14	429.68*	41.30	213.49	15.73	1.27
	Eosin yellowish	6.28	414.59	41.31	215.56	15.63	1.07

Among FF fill factor ratios of DSSCs, Black Mulberry having a coating cycle of 10 cycles is the maximum. Power conversion efficiency of dye sensitizer solar cells is also seen in the table.

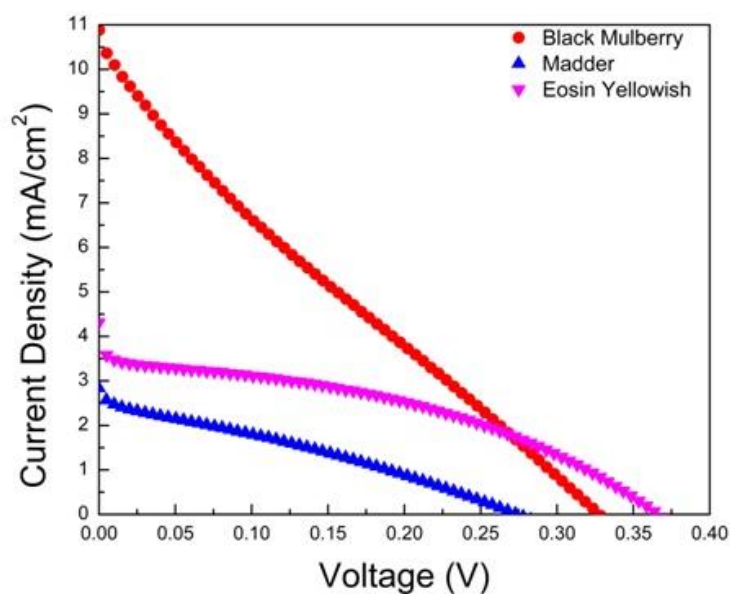


Figure 4. 8 J-V curve for DSSC with different dyes for 5 coating cycles

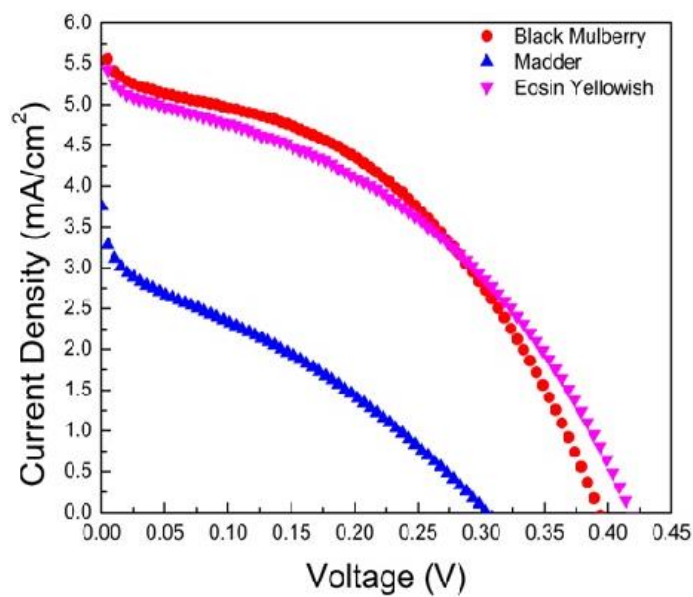


Figure 4. 9 J-V curve for DSSC with different dyes of for 10 coating cycles

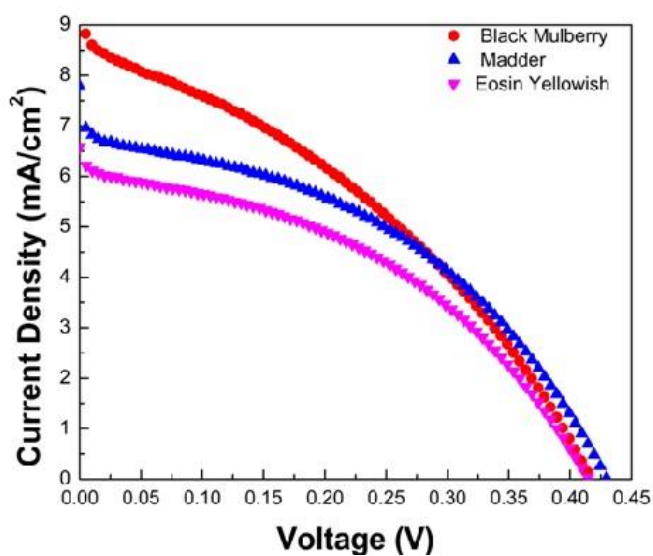


Figure 4. 10 J-V curve for DSSC with different dyes for 15 coating cycles

When calculated according to the formula $\eta = (V_{OC} \times J_{SC} \times FF)/P_{in}$, 15 cycles coated TiO_2 with loading of Black Mulberry having 1.30% efficiency has the highest efficiency.

CHAPTER 5

DISCUSSION AND CONCLUSION

Table 1 shows the photovoltaic characteristic parameters found by *JV* measurements for the investigated samples. Where J_{sc} , V_{oc} , FF , R_s , R_{SH} are the open circuit current density, the open circuit voltage, the fill factor, the series resistance of the equivalent circuit, and the parallel resistance of the equivalent circuit, respectively. Depending on dyes used and varying thickness of samples affect all these parameters. The variance in J_{sc} generally is related closely to two parameters. The first one is ability of the photoanode to absorb light, and secondly to the electron diffusion distance. For high J_{sc} , it is desirable that the absorption ability is large and the diffusion distance is small. Generally, as the absorption capacity increases with increasing sample thickness, the electron diffusion distance decreases. Therefore, there is competition between these two factors. As seen in Table 1, except for 5-layer sample loaded black mulberry, when the samples are taken into consideration, it has been seen that J_{sc} always increases with the thickness. Absorbance plots in the visible region were measured after dyeing for each sample. Accordingly, a 5-layer black mulberry in the visible region appears to have an extraordinary peak at around 550 nm, indicating that the peak absorbance value is unusually high. This shows that it can be benefited from the photons of long wavelength, and thus the J_{sc} value is high. While there was no peak before the dye loading, after the dye loading both the ability of absorption increased and the peaks in the long wavelength increased. Considering the V_{oc} behavior in all the other samples, the first factor shows that it is more dominant than the second one .

$$V_{oc} = \left(\frac{k_B T}{q}\right) \ln \left(\frac{I_{inj}}{I_r}\right) \quad (2.12)$$

The formula for V_{oc} is given by equation (2.12) [64] . The I_{inj} in this formula is due to the electrons from the stimulated dye. I_r represents the recombination current. Other constants q , T , k_B are the electron charge, absolute temperature, the Boltzmann constant, respectively. The reason why V_{oc} shows different values for different dyes is because of the change of I_{inj} [64]. With improving thickness, enhancement of I_{inj}

is expected because of the ability to absorb with increasing thickness, the number of excited electrons from the dye increases. The I_r current is related to the recombination of the electron-hole pair. With increasing thickness, the carrier transport length extends. This extension brings about the probability of recombination. In this study V_{oc} is always increased with thickness. The reason for this is that with increasing thickness, the change of I_{inj} is faster than that of I_r . The measured R_s and R_{sh} values directly affect the FF . As it is well known, it is desirable for R_{sh} to be large, R_s to be small for the high fill factor. The 5-layer black mulberry R_{sh} value is much smaller than the other dyes. This causes the FF to fall. Looking at the other two 5-layer samples, the FF value in eosin-y is also greater than that of madder because R_s and R_{sh} are due to further improvement. When 10-layers of samples are examined, the smallest R_s and the largest R_{sh} belong to black mulberry. This is followed by eosin-y and madder, respectively, so the FF value is the best in the black mulberry. When the 15-layer samples are analyzed, R_s values are very close to each other, so R_{sh} values determine FF . The smallest R_{sh} belongs to the black mulberry, and therefore the FF value of black mulberry is the lowest. Since the R_{sh} values of Madder and eosin are close to each other, the FF values are almost the same.

As it is well known, the most commonly used dye in DSSCs is ruthenium. But the cost of ruthenium is high, so in this study, fruit dyes and eosin were preferred although their performance is low. When the photovoltaic conversion efficiency is investigated, since the efficiency value is calculated with the equation (2.9), the multiplication of I_{sc} , V_{oc} and FF leads to an increase in the efficiency value. Variations in dye and thickness have led to increased efficiency. It was found that the best dye was black mulberry among others in terms of efficiency. Increased sample thickness led to improvement efficiency for all coatings cycles. It was also figured out that the effect of the other dyes on efficiency, with increasing thickness, approached the performance of black mulberry. It was observed that the efficiency of eosin was closer to black mulberry when it was increased from 5 cycles to 10 cycles, and when madder was increased from 10 cycles to 15 cycles, there was a dramatic increase in performance. Mulberry fruit seems to have ingredients containing anthocyanins which has good chemical bonding with TiO_2 [65]. Specially, cyanine

contributing to fruit red pigment from red to purple color which (structure presented here in) is known to contain. In the extracts of natural fruit, the black mulberry extract performed the best photosensitized effect, which was due to the better interaction between the carbonyl and hydroxyl groups of anthocyanin molecule on black mulberry extract and the surface of TiO₂ porous film [66]. The DSSC obtained with mulberry shows the best performance among the other extracts investigated, thus this indicates that anthocyanins in this extract inject electrons more efficiently than other species used. A large number of solar cells produced using mulberry are not available in the literature. However, in an earlier study of mulberry, a value of about 1.6% efficiency was obtained [67]. In another study using mulberry fruit extracts, a efficiency of approximately 0.6% was found [68]. The energy conversion efficiency that we achieved is also consistent with these values. Consequently, the best result was found to belong to the black mulberry sample having 15-layer with 1.3% efficiency.

REFERENCES

- [1] N. S. Lewis, *Science* 315-798, 2007.
- [2] Grätzel, M., “Solar Energy Conversion by Dye-Sensitized Photovoltaic Cells”, *Inorg.Chem.*, 44(20), 6841–6851, 2005.
- [3] Shah, A., Torres, P., Tscharnner, R., et al. “Photovoltaic technology: The case for thin-film solar cells”. *Science*, , 285: 692–698, 1999.
- [4] Choubey¹, P.C., Oudhia, A. and Dewangan, R, “A review: Solar cell current scenario and future trends.”, *Recent Research in Science and Technology*, 4(8): 99-101, 2012.
- [5] Pekkola, R., “Electronic Structure of Solid-State Dye-Sensitized Solar Cells: Synchrotron Induced Photoelectron Spectroscopy on Nanocrystalline TiO₂, Newly Developed Dyes and Spiro-MeOTAD”, Doctor Thesis, Technische Universität Darmstadt, 2014.
- [6] Green, M. A., Emery, K., Hishikawa, Y., Warta, W., and Dunlop, E. D., “Progress in Photovoltaics.” 20,12, (2012).
- [7] O'Regan, B. and Gratzel, M., “A low-cost, high-efficiency solar cell based on dye-sensitized colloidal TiO₂ films”, *Nature*, 353(6346): p. 737-740., 1991.
- [8] Shah , A., [http:// www.greenworldinvestor.com/2011/07/04/dye-sensitised-solar-cells-dscc-processadvantages-and-disadvantages/](http://www.greenworldinvestor.com/2011/07/04/dye-sensitised-solar-cells-dscc-processadvantages-and-disadvantages/) [Access date: September 2017].
- [9] JianFeng, LU., Jie, BAI., XiaoBao, XU., ZhiHong, LI., Kun, CAO., CUI Jin & WANG MingKui* “Alternate redox electrolytes in dye-sensitized solar cells”, 2012.
- [10] Tuller, H. L., “Solar to fuels conversion technologies: a perspective” *Mater Renew Sustain Energy*; 6(1): 3, 2017.

- [11] Maçaira, B. J., Mesquita, I., Andrade, L., Mendes, A., "Role of temperature in the recombination reaction on dye-sensitized solar cells", 2015
- [12] Stathatos, E., "Dye Sensitized Solar Cells as an Alternative Approach to the Conventional Photovoltaic Technology Based on Silicon - Recent Developments in the Field and Large Scale Applications," Solar Cells - Dye-Sensitized Devices, Chapter 21, 2011.
- [13] Sewvandi, G. A., "Interface and Structural Engineering of DyeSensitized Solar Cells and Perovskite Solar Cells for High Efficiencies", Doctoral degree, 2015.
- [14] Afzaal, M., Yates, H. M. and Hodgkinson, J. L., "Translation Effects in Fluorine Doped Tin Oxide Thin Film Properties by Atmospheric Pressure Chemical Vapour Deposition", 2015.
- [15] Pugliese, D., "New insights in Dye-sensitized Solar Cells: novel nanostructured photoanodes, metal-free dye, quasi-solid electrolytes and physics-based modeling", PhD thesis, 2014.
- [16] Mahmood, K., Sarwarb, S. and Mehranb, M. T., "Current status of electron transport layers in perovskite solar cells: materials and properties", *Coatings* 6(4), 43; 2016.
- [17] Sharma, A., Karn, R.K. , Pandiyan, S. K., "Synthesis of TiO₂ Nanoparticles by Sol-gel Method and Their Characterization", *Journal of Basic and Applied Engineering Research*, Volume 1, Number 9, 2014.
- [18] Ariyasinghe, D. M. B. P.," Improved performance of dye-sensitized solar cells using a diethyldithiocarbamate-modified TiO₂ surface", *Journal of Nanomaterials*, Article No. 57, 2013.
- [19] El-Agez, M., Taher , T., Elrefi, S. S., Monzir, A. L., " Dye-sensitized solar cells using some organic dyes as photosensitizers", *Optica Applicata*. 44. 345-351, 2014.

- [20] Ameen, S., Akhtar, M. S., Song, M. and Shin, H. S., "Metal Oxide Nanomaterials, Conducting Polymers and Their Nanocomposites for Solar Energy, Chapter 8, 2013.
- [21] Mathewa, A., Ananda, V., RAO, G. M., Munichandraiah, N., "Effect of iodine concentration on the photovoltaic properties of dye sensitized solar cells for various I₂/LiI ratios", *Electrochimica Acta* 87-92–96, 2013.
- [22] Kinhal, K., "Effects of Sputtered Platinum Counter Electrode and Integrated TiO₂ Electrode with SWCNT on DSSC Performance", Masters Thesis, 2011.
- [23] Seery, M., <https://photochemistry.wordpress.com/2009/08/24/light-absorption-and-fate-of-excited-state/> [Access date: November 2017].
- [24] Lee, J.J. & Rahman, Md & Sarker, Subrata & Nath, Narayan Chandra Deb & Ahammad, A. J. Saleh & Lee, J.K., "Metal oxides and their composites for dye-sensitized solar cells", *Advances in Composite Materials for Medicine and Nanotechnology*. 181-201, 2011.
- [25] Siu, C. H., "Metallated and metal-free molecular dyes for dye-sensitized solar cells" *Hong Kong Baptist University*, Doctor of Philosophy (PhD),, 2014.
- [26] Barr, T. J., "Interfacial Electron Transfer At Sensitized Nanocrystalline TiO₂ Electrolyte Interfaces: Influence Of Surface Electric Fields And Lewis-Acidic Cations" University of North Carolina, Degree of Doctor of Philosophy in the Department of Chemistry, 2017.
- [27] Theerthagiri, J., Senthil, A. R., Madhavan, J. and Maiyalagan, T., "Recent Progress in Non-Platinum Counter Electrode Materials for Dye-Sensitized Solar Cells", *ChemElectroChem* 2, 928 – 945, 2015.
- [28] Grätzel, M., "Review Dye-sensitized solar cells", *Journal of Photochemistry and Photobiology C: Photochemistry Reviews* 4 -145–15, 2003.
- [29] <http://www.alternative-energy-tutorials.com/energy-articles/solar-cell-i-v-characteristic.html> [Access date: November 2017].

- [30] shodhganga.inflibnet.ac.in/bitstream/10603/23334/9/09_chapter%202.pdf
[Access date: November 2017].
- [31] El-Refi, K. S., "Dye-Sensitized Solar Cells Using TiO₂ as a Semiconducting Layer", B.Sc. in Physics, Islamic University of Gaza, Master Degree, 2013.
- [32] Yong, H., "Design and synthesis of new organic dyes for highly efficient dye-sensitized solar cells (DSSCs)", Hong Kong Baptist University, Degree of PhD, 71, 2014.
- [33] Moody, B. F., "Strained Layer Superlattice Solar Cells", A dissertation submitted to the Graduate Faculty of North Carolina State University, 2006.
- [34] Imran, K. M., "A Study on the Optimization of Dye-Sensitized Solar Cells", Graduate Theses and Dissertations, University of South Florida, Degree of Master, 2013.
- [35] Ariyasinghe, D. M. B. P., "Improved performance of dye-sensitized solar cells using a surface modified TiO₂ electrode", Shizuoka university, Doctor Thesis, 2013.
- [36] newworldencyclopedia.org/entry/File:Solar_cell_equivalent_circuit.svg
[Access date: December 2017].
- [37] David Garrido Diez "Electric Measurements On Crystalline Silicon Concentration Cells", Slovak University Of Technology, Diploma Thesis, 2008.
- [38] <http://www.iust.ac.ir/find.php?item=74.11421.21690.en>
[Access date: December 2017].
- [39] Yimhyun, J., "Study on Dye Sensitized Solar Cells for Improved Performances", A dissertation submitted to the Graduate School of UNIST in partial fulfillment of the requirements for the degree of Doctor of Philosophy, 2014.

- [40] http://www.newworldencyclopedia.org/entry/Solar_cell#Shunt_resistance
[Access date: November 2017].
- [41] Elnugoumi, M. G., Zainal, A. A., and Mahmoud Kh. Mahmoud A., “Current status and Challenges of Solar Energy in Malaysia; A Review” , Journal of Advanced Science and Engineering Research Vol 2, 2011.
- [42] <https://www.renewableenergyhub.co.uk/solar-panels/the-history-of-solar-energy-and-solar-panels.html> / [Access date: October 2017].
- [43] https://www1.eere.energy.gov/solar/pdfs/solar_timeline.pdf
[Access date: October 2017].
- [44] http://ethw.org/Milestones:First_Practical_Photovoltaic_Solar_Cell
[Access date: October 2017].
- [45] https://ocw.tudelft.nl/wp-content/uploads/solar_energy_section_11.pdf
[Access date: October 2017].
- [46] Jones, G., Bouamane, L., “Power from Sunshine”: A Business History of Solar Energy”, Harvard Business School, 2012.
- [47] Honda, H., Ishizaki, A., Soma, R., Hashimoto, K., and Fujishima, A., “Application of photocatalytic Reactions caused by TiO₂ film to improve the maintenance factor of lighting systems”, *J.Illum.Eng.Soc.Winter*, 42-49., 1998.
- [48] Hagfeldt, A., Grätzel M., *Acc. Chem. Res.*, 33 pp. 269-277., 2000.
- [49] Lee, K. M., Suryanarayanan, V., Chuan, K. H. “The influence of surface morphology of TiO₂ coating on the performance of dye-sensitized solar cells”, *Solar Energy Materials and Solar Cells* Volume 90, Issue 15, 2006.
- [50] Ito, S., Nazeeruddin, M.K., Zakeeruddin, S.M., Ichiyama, P. P., Comte, P., Grätzel, M., Mizuno, T., Tanaka, A., and Koyanagi, T., “Study of Dye-Sensitized Solar Cells by Scanning Electron Micrograph Observation and

- Thickness Optimization of Porous TiO₂ Electrodes”, *International J. Photoenergy*, 517609, 2009.
- [51] Alhamed, M., Issa, A. S., Doubal, A. W., “Studying Of Natural Dyes Properties As Photo-Sensitizer For Dye Sensitized Solar Cells (Dssc)”, *Journal of Electron Devices*, Vol. 16, pp. 1370-1383, 2012.
- [52] Kakiage, K., Aoyama, Y., Yano, T., Oya, K., Kyomen, T., and Hanaya, M., “Fabrication of a high-performance dye-sensitized solar cell with 12.8% conversion efficiency using organic silyl-anchor dyes”, *Chem. Commun.*, 51, 6315-6317, 2015.
- [53] Kakiage, K., Aoyama, Y., Yano, T., Oya, K., Fujisawa, J. and Hanaya, M., “Highly-efficient dye-sensitized solar cells with collaborative sensitization by silyl-anchor and carboxy-anchor dyes” ,*Chem. Commun.*, DOI: 10.1039, 2015.
- [54] <http://merlab.metu.edu.tr/tr/x-isini-difraktometresi>
[Access date: December 2017].
- [55] Hasançebi, Ö., “Sol-Gel Yöntemiyle Hazırlanan Bakır Oksit İnce Filmlerin Elektriksel, Yapısal Ve Optiksel Özelliklerinin İncelenmesi” Master Thesis., Ankara University, 2006.
- [56] <https://publish.illinois.edu/x-raycrystallography/2014/12/18/introduction/>
[Access date: December 2017].
- [57] <http://www.bragitoff.com/2017/08/x-ray-diffraction-xrd/>
[Access date: December 2017].
- [58] <https://www.slideshare.net/MdAtaulMamun/introduction-to-atomic-force-microscopy> [Access date: December 2017].
- [59] <http://Inf-wiki.eecs.umich.edu/wiki/AtomicForceMicroscopy/>
[Access date: December 2017].
- [60] <https://bilimfili.com/atomik-kuvvet-mikroskobu-nedir-nasil-calisir/>
[Access date: December 2017].

- [61] faculty.sdmiramar.edu/fgarces/labmatters/instruments/uvvis/cary50.htm
[Access date: December 2017].
- [62] www.shimadzu.com/an/uv/support/fundamentals/monochromators.html/
[Access date: December 2017].
- [63] <http://abet-technologies.com/solar-simulators/solar-simulator-elements/>
[Access date: December 2017].
- [64] Ko, Y. S., Kim, M. H., and Kwon, Y. U., "Method to Increase the Surface Area of Titania Films and Its Effects on the Performance of Dye-Sensitized Solar Cells", *Bull. Korean Chem. Soc.*, Vol. 29, No. 2, 2008.
- [65] Kalaivani, J., Renukadevi, K., Ramachandran, K., Srinivasan, R., "TiO₂ based dye-sensitized solar cell using natural dyes" *Nanosystems: Physics, Chemistry, Mathematics*, 2016.
- [66] Sutikno, Afrian, N., Supriadi, Putra, N.M.D., "Synthesis and Characterization of Allium Cepa L. as Photosensitizer of Dye-Sensitized Solar Cell" , *AIP Conference Proceedings*, 2016.
- [67] Patrocínio, A.O.T., Mizoguchi, S.K., Paterno, L.G., Garcia, C.G., Murakami, N.Y., "Efficient and low cost devices for solar energy conversion: Efficiency and stability of some natural-dye-sensitized solar cells" *Synthetic Metals*, 2009.
- [68] Chang, H. & Yu-Jen, L., "Pomegranate leaves and mulberry fruit as natural sensitizers for dye-sensitized solar cells", *Solar Energy - SOLAR ENERG.* 84. 1833-1837. 10.1016/j.solener, 2010.

CURRICULUM VITAE

PERSONAL INFORMATION

Name Surname : Zikreddin Kerem YILDIZ
Date of Birth : 1984
Phone : +90 541 295 69 68
E-mail : keremyildiz84@hotmail.com



EDUCATION

High School :Sincan High School/ANKARA
(4.37/5) (1999-2001)
Bachelor : Kırıkkale University /KIRIKKALE (2002-2007)
(2.66/4.0)
Master Degree :Ankara Yıldırım Beyazıt University / (2015-continued)

WORK EXPERIENCE

Field Chief : Selen-Y Elektrik A.Ş (2008-2009)
Field Chief : PTT A.Ş (2009-2010)
Subcontract Administrator : TRT-Turkish Radio and Television Corporation
(2010- continued)

TOPICS OF INTEREST

- Broadcasting
- Nano technology
- Dye Sensitized Solar Cell